

Bioinspiration & Biomimetics



PAPER

Lift calculations based on accepted wake models for animal flight are inconsistent and sensitive to vortex dynamics

RECEIVED
7 June 2016

REVISED
2 November 2016

ACCEPTED FOR PUBLICATION
4 November 2016

PUBLISHED
6 December 2016

Eric Gutierrez^{1,2,3}, Daniel B Quinn¹, Diana D Chin¹ and David Lentink¹

¹ Department of Mechanical Engineering, Stanford University, Stanford, CA 94305, USA

² Department of Aeronautics and Astronautics, Stanford University, Stanford, CA 94305, USA

³ Author to whom any correspondence should be addressed.

E-mail: eguti007@gmail.com

Keywords: animal flight, flapping wing, vortex wake, stereo particle image velocimetry, quasi-steady lift, model, validation

Supplementary material for this article is available [online](#)

Abstract

There are three common methods for calculating the lift generated by a flying animal based on the measured airflow in the wake. However, these methods might not be accurate according to computational and robot-based studies of flapping wings. Here we test this hypothesis for the first time for a slowly flying Pacific parrotlet in still air using stereo particle image velocimetry recorded at 1000 Hz. The bird was trained to fly between two perches through a laser sheet wearing laser safety goggles. We found that the wingtip vortices generated during mid-downstroke advected down and broke up quickly, contradicting the frozen turbulence hypothesis typically assumed in animal flight experiments. The quasi-steady lift at mid-downstroke was estimated based on the velocity field by applying the widely used Kutta–Joukowski theorem, vortex ring model, and actuator disk model. The calculated lift was found to be sensitive to the applied model and its different parameters, including vortex span and distance between the bird and laser sheet—rendering these three accepted ways of calculating weight support inconsistent. The three models predict different aerodynamic force values mid-downstroke compared to independent direct measurements with an aerodynamic force platform that we had available for the same species flying over a similar distance. Whereas the lift predictions of the Kutta–Joukowski theorem and the vortex ring model stayed relatively constant despite vortex breakdown, their values were too low. In contrast, the actuator disk model predicted lift reasonably accurately before vortex breakdown, but predicted almost no lift during and after vortex breakdown. Some of these limitations might be better understood, and partially reconciled, if future animal flight studies report lift calculations based on all three quasi-steady lift models instead. This would also enable much needed meta studies of animal flight to derive bioinspired design principles for quasi-steady lift generation with flapping wings.

List of symbols

A_d	vortex ring area	I_z	vertical impulse of the vortex ring
A_p	projected area of the vortex ring	J	advance ratio
b	wingspan	L	lift
b_w	span of the wake	L_{AD}	lift based on the actuator disk model
c	average wing chord length	L_{KJ}	lift based on the Kutta–Joukowski theorem
c_a	wake-vortex added mass coefficient	L_{VR}	lift based on the vortex ring model
f	wingbeat frequency		

l_v	diameter of the vortex structure
m	body mass of the bird
\dot{m}	mass flux through the vortex ring
N	number of bird individuals
n	number of flights per bird
R	root-to-tip wing length
St	Strouhal number
T	duration of the downstroke during which a vortex ring is created
t	time
U	bird's body velocity
U_{eff}	average effective wing speed
U_v	convection velocity of the vortex
U_∞	wind tunnel speed
\bar{u}, \bar{w}	horizontal and vertical velocities of the flapping wing
W	bodyweight
w	average downwash at the vortex ring
W_a	wake vortex ratio
w_{vo}	initial wingtip vortex diameter
w_w	window width used by the vortex tracking algorithm
x, y, z	rectangular coordinates of the bird's flight path
ρ	air density
Γ	vortex circulation
λ	total length of the vortex ring
θ	stroke plane angle
ϕ	full wingbeat amplitude

1. Introduction

Freely flying animals shed well-defined vortices in their wakes, which are shaped by the aerodynamic lift forces generated by the wings and body. Our understanding of how insects, bats, hummingbirds, and other birds create these 'aerodynamic footprints' has been advanced by early particle tracking velocimetry measurements (e.g. Spedding *et al* 1984), and more recent Particle Image Velocimetry (PIV) flow measurements (e.g. Spedding *et al* 2003, Rosén *et al* 2007, Hubel *et al* 2009, Muijres *et al* 2011a, Kirchhefer

et al 2013, Wolf *et al* 2013, Håkansson *et al* 2015). The majority of recent studies have been performed in wind tunnels where the vortices advect downstream through a laser sheet positioned a few wing chord lengths downstream of the animal (e.g. Hedenström *et al* 2006b, Henningsson *et al* 2015). This approach, however, cannot capture the three-dimensional process of vortex formation in the vicinity of the wing or any deformation that occurs before the vortex wake advects into the laser sheet (Bomphrey *et al* 2012). Instead, it is typically assumed that the shape and strength of the vortex wake do not change as it advects downstream, which is referred to as 'the frozen turbulence hypothesis'. This assumption helps justify the application of three widely used quasi-steady aerodynamic models to calculate lift based on the measured wake: the Kutta–Joukowski theorem (Hedenström *et al* 2006a, Hubel *et al* 2010, Henningsson and Hedenström 2011, Henningsson *et al* 2011, Muijres *et al* 2011b), the vortex ring model (Hedenström *et al* 2006a, Henningsson *et al* 2008, Johansson *et al* 2008, Johansson *et al* 2012, Wolf *et al* 2013), and the actuator disk model (Muijres *et al* 2011a, Muijres *et al* 2012b, Håkansson *et al* 2015). The lift is considered quasi-steady in these studies based on the assumption that the majority of the lift is generated by the instantaneous flow field for every phase of the wingbeat (Sane 2003). These models tend to underestimate the lift needed to support bodyweight, most notably the Kutta–Joukowski theorem (Tian *et al* 2006, Henningsson *et al* 2008, Hubel *et al* 2010, Hubel *et al* 2012) and vortex ring model (Spedding *et al* 1984, Spedding 1986, Spedding *et al* 2003, Hedenström *et al* 2006a, Henningsson *et al* 2008).

There are various hypotheses that may explain lift underestimation. For example, it is possible that the vortex structures partially break down due to interactions with background turbulence, or other vortex structures shed by the animal (Hubel *et al* 2009). Indeed, during a seminal study with pigeons flying slowly in still air, Spedding *et al* (1984) found that the vortex rings produced during the downstroke of previous wingbeats were affected by subsequently generated vortex rings. Another possibility is that a significant fraction of the vortex sheet shed by the wing may be undetectable due to diffusion before it is gathered up into the primary tip vortex (Hubel *et al* 2009). Additionally, some circulation may not be fully captured due to sub-optimal laser energy, seeding density, and spatial resolution (Hubel *et al* 2010, Waldman and Breuer 2012). Another potential explanation is Crow instability, which could decrease the measured wake span and the calculated weight support (Henningsson *et al* 2011, Horstmann *et al* 2014). Finally, omitting the unsteady 'added mass' effects due to the acceleration of vortices might further increase the underestimation of lift (Dabiri 2005). To avoid such errors, it has been proposed that added mass effects can be omitted if the

dimensionless wake vortex ratio, $W_a = c_a l_v U_v / \Gamma$, is below a critical value, $W_a = 0.42$, which is calculated as $c_a / (1 + c_a)$ (Dabiri *et al* 2006), with $c_a = 0.72$ being the wake-vortex added mass coefficient, l_v the diameter of the vortex structure in the direction of propagation, U_v the convection velocity of the vortex, and Γ the circulation of the vortex (Dabiri 2005). Hedenström *et al* (2006b) calculated $W_a = 0.06$ for a thrush nightingale flying at its slowest flight speed of 4 m s^{-1} and thus concluded that added mass effects could be ignored.

A number of studies have made strides to derive aerodynamic models that are able to more accurately estimate the forces generated by wings (Noca *et al* 1997, Noca *et al* 1999, Dabiri 2005, Mohebbian and Rival 2012, Wang *et al* 2013, Gemmell *et al* 2015). However, primarily due to a lack of 3D time and space resolved velocity data needed to apply these formulations, most animal flight studies still rely on simplified quasi-steady lift models. Dabiri (2005) identified many invalid assumptions in these popular lift models. These assumptions cause phase and amplitude errors that were confirmed by Computational Fluid Dynamics studies (Minotti 2011, Wang *et al* 2013), which significantly limit the accuracy of these quasi-steady lift formulations for flapping wings (Wang *et al* 2013, Liu *et al* 2015, Wang *et al* 2015). Similarly, these limitations apply to the flapping wings of micro air vehicles (Garrick 1936, Young 2005, Shyy *et al* 2008, Gopalan and Povitsky 2010, Ol 2010, Shyy *et al* 2013). Although it is known that simple quasi-steady aerodynamic models can lead to inaccurate lift estimates, an experimental study that compares the lift predicted by these different models for a single data set is needed to help determine the extent to which results across animal flight studies can be used reliably for comparative analyses. Furthermore, these models need to be compared both close to the animal (near wake) and further downstream (far wake), while making sure downstream wake development is not impeded by background turbulence. Such comparisons are helpful for designing future meta studies to derive design principles for lift generation inspired by flapping animal flight.

To determine how the various wake-based lift models compare, we measured the wake development of a bird flying through a laser sheet in still air. This requires an additional level of laser safety for the bird compared to previous studies. Earlier safety measures included placing a light curtain upstream of the laser sheet (Spedding *et al* 2003, Hubel *et al* 2009, Hubel *et al* 2010), a light filter mask around feeders (Hedenström *et al* 2006b, Muijres *et al* 2008, Muijres *et al* 2014), or triggering the laser sheet once the animal safely traveled beyond the laser sheet (Tian *et al* 2006, Hubel *et al* 2012, Muijres *et al* 2012b, Ben-Gida *et al* 2013, Kirchhefer *et al* 2013). Some studies used custom-made miniature bird goggles to protect the bird's eyes from direct contact with laser light (Muijres

et al 2012a, Ben-Gida *et al* 2013, Kirchhefer *et al* 2013), such as using thin theater filters originally developed for other purposes. To ensure the bird's laser safety, we developed advanced laser safety goggles for a bird and trained it to fly voluntarily through the laser sheet while wearing these laser safety goggles. Based on the wake data, we evaluated the predictive performance of the three commonly used quasi-steady lift models. By permutating the different ways of calculating model parameters used in the literature, we determined how different parameter definitions and calculations influence the predicted lift outcome. Therefore, our comparison on a single dataset provides valuable insight into how different models and model parameter choices might affect quasi-steady lift estimates across the animal flight literature.

2. Methods

2.1. Still air bird flight experiments and bird training

We trained a Pacific parrotlet to fly through a laser sheet oriented transverse to the flight path in the middle of two perches (figures 1(a), (b)). The enclosed flight volume used for these flow recordings was $\sim 3 \text{ m}$ long, $\sim 2 \text{ m}$ high, and $\sim 1.5 \text{ m}$ wide. The two perches were located 1 m apart at $\sim 0.8 \text{ m}$ above the ground, and the centerline of the laser sheet was positioned $\sim 0.9 \text{ m}$ above the ground. After five flights through the laser sheet to optimize PIV settings based on the measured airflow, we recorded three flights (*Forpus coelestis*; mass $m = 29 \text{ g}$; wingspan $b = 0.21 \text{ m}$; wingbeat frequency $f = 23 \text{ Hz}$; full wingbeat amplitude $\phi = 103^\circ$ (1.8 radians); $N = 1$ bird; $n = 3$ flights). In the first recording, seeding density varied, facilitating flow visualization, and for the second and third flights we realized uniform seeding. The measured average speed of the parrotlet's head, U , was 1.75 , 1.50 , and 1.75 m s^{-1} for the first, second, and third flight, respectively. The advance ratio was on average approximately $J \approx 0.2$ across the three flights ($J = U/2\phi fR$, where $R = 0.09 \text{ m}$ is the approximate root-to-tip wing length and ϕ is in radians). The bird took off voluntarily and flew at near constant speed through the laser sheet to the landing perch when the trainer pointed (cue). We trained this behavior using positive reinforcement (Skinner 1938, McGreevy and Boakes 2011) with a clicker as the bridge and millet seed as the reward. Before and after training, the bird was fed Roudybush Daily Maintenance and water *ad libitum* (its diet also included fresh broccoli). Training required several months of effort with a cohort of four individuals, of which only one bird flew voluntarily in our setup while wearing laser goggles. The parrotlet became accustomed to wearing these goggles through many small stress-free steps of habituation and training that approximated the flight. All training and experimental procedures were approved by Stanford's Administrative Panel on Laboratory Animal Care.

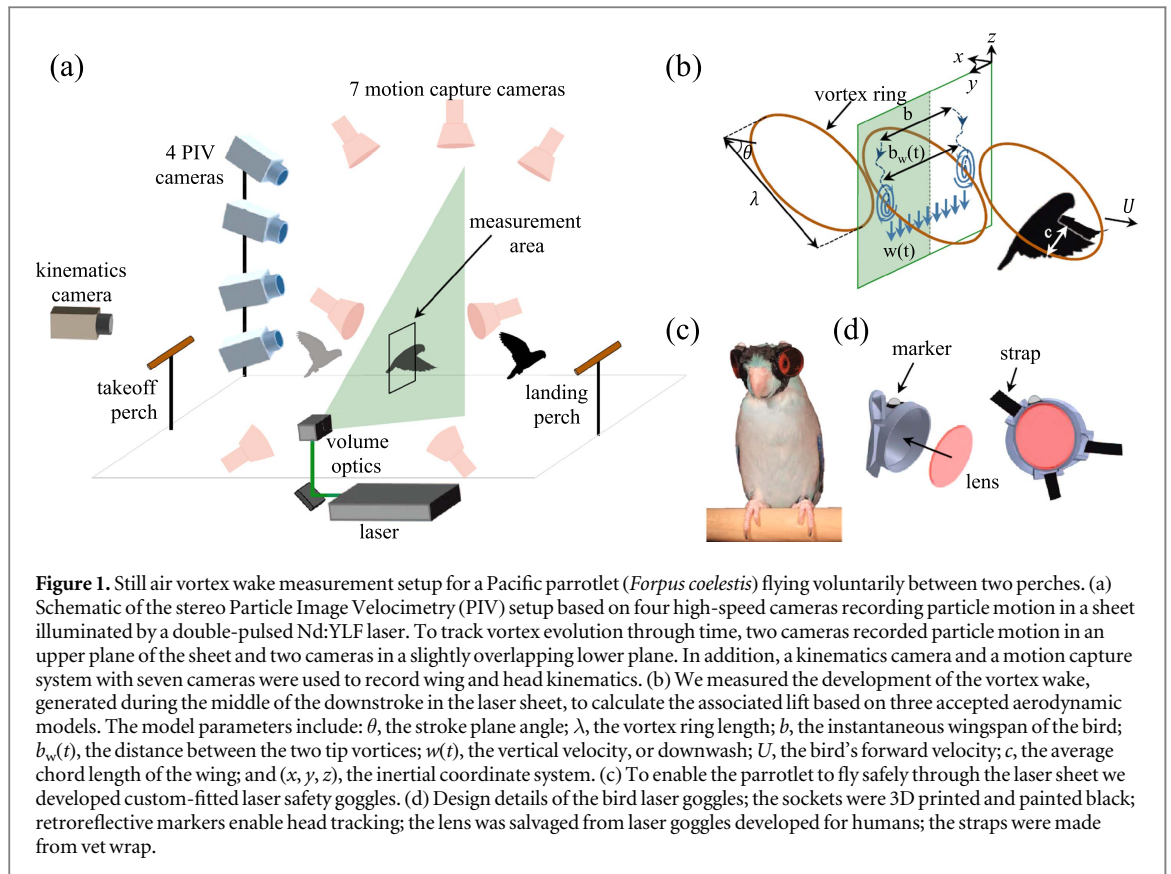


Figure 1. Still air vortex wake measurement setup for a Pacific parrotlet (*Forpus coelestis*) flying voluntarily between two perches. (a) Schematic of the stereo Particle Image Velocimetry (PIV) setup based on four high-speed cameras recording particle motion in a sheet illuminated by a double-pulsed Nd:YLF laser. To track vortex evolution through time, two cameras recorded particle motion in an upper plane of the sheet and two cameras in a slightly overlapping lower plane. In addition, a kinematics camera and a motion capture system with seven cameras were used to record wing and head kinematics. (b) We measured the development of the vortex wake, generated during the middle of the downstroke in the laser sheet, to calculate the associated lift based on three accepted aerodynamic models. The model parameters include: θ , the stroke plane angle; λ , the vortex ring length; b , the instantaneous wingspan of the bird; $b_w(t)$, the distance between the two tip vortices; $w(t)$, the vertical velocity, or downwash; U , the bird's forward velocity; c , the average chord length of the wing; and (x, y, z) , the inertial coordinate system. (c) To enable the parrotlet to fly safely through the laser sheet we developed custom-fitted laser safety goggles. (d) Design details of the bird laser goggles; the sockets were 3D printed and painted black; retroreflective markers enable head tracking; the lens was salvaged from laser goggles developed for humans; the straps were made from vet wrap.

2.2. Bird laser safety goggles

We developed bird laser safety goggles that were custom-fit and built for the parrotlet to protect its eyes during the PIV experiments (figures 1(c), (d)). The goggle sockets were 3D printed (ProJetTM HD 3500) from clear acrylic material (VisiJet[®] Crystal) and painted with carbon black acrylic paint (Golden Fluid Acrylics). The lenses were salvaged from professional laser safety goggles with polycarbonate filter lenses of optical density 6. The lenses were cut to size and friction fit to the goggle sockets. The goggle sockets were wrapped around the bird's head with three pieces of lightweight, self-stick Vetrap Bandaging Tape. The goggles covered the entire eyes of the bird from any direct or stray laser light and could not be taken off by the bird during the experiments. To prevent the goggles from fogging up, we applied a thin film of shaving cream (Barbasol) onto the surface of the lenses. The total weight of the goggles was 1.68 grams, about 5.8% of the bird's mass (sockets, 0.44 g; lenses, 0.68 g; vet wrap, 0.14 g; paint, 0.34 g; reflective markers, 0.08 g). See electronic supplementary materials for 3D CAD models of the laser safety goggle design.

2.3. Flow field, wingbeat, and flight speed measurements

We used wide-field high-speed stereo PIV to measure the evolution and breakdown of the vortices in the wake of the bird, and we measured the bird's kinematics using a high-speed camera and motion capture system (figure 1(a)). All recordings were

synchronized at 1000 Hz. We created two overlapping stereo flow field recordings using two pairs of high-speed cameras. The stereo compositions were stitched together in the vertical direction using the stitching tool in DaVis 8.2.2 (PIV Software, LaVision, Göttingen, Germany). We recorded 4000 frames per flight and analyzed about 167 frames per flight on average. Each frame covered an area approximately 240 mm high and 230 mm wide and captured the wake produced by the right side of the bird's body and wing. We constructed the flow field spanning from the left to right wingtip by mirroring the measured wake of the right wing similar to earlier animal wake studies. We checked the validity of the symmetry assumption using the four cameras in a planar configuration distributed over both the width (2 cameras) and height (2 cameras) of the wake generated by the left and right wing (of another parrotlet individual from the same colony). This pilot experiment showed that the vortex wake can become asymmetric (see supplementary figure S1). Nevertheless, we chose to focus on recording half of the wake, because we found that stereo PIV was required for accurate frame stitching when multiple cameras were used. The flow in the flight arena was seeded with a colorless and odorless fog (aerosol liquid, particle size $1 \mu\text{m}$, di-ethyl-hexyl-sebacat) for 30 s approximately 2 min before each recorded flight (particle seeder, LaVision). The mist is non-toxic and appears to have no effect on the bird's behavior. The particles were illuminated with a 5.5 mm thick laser sheet set perpendicular to the bird's flight direction

using a double-pulsed Nd:YLF laser (Litron LDY304; 527 nm; 1000 Hz; 30 mJ per laser head per pulse; Bozeman, MT, USA). Pairwise images ($dt = 200 \mu\text{s}$) were recorded using four high-speed cameras (Phantom Miro M310; 1000 Hz; 1280×800 pixels; 12 bits; sensor size of 25.6×16.0 mm). The PIV cameras were equipped with 100 mm lenses (Tokina AF 100 mm F2.8: AT-X 100 PRO D) set to aperture 4. The cameras viewed the light sheet obliquely from an angle using Scheimpflug mounts (LaVision) to tilt the focal plane. The system was operated using DaVis 8.2.2. A fifth high-speed camera (Phantom Miro LC310; color) filmed the bird from behind to record the bird's wingstroke angle and position in the laser sheet during flights 2 and 3. Body speed was measured by tracking two lightweight retro-reflective markers (half-sphere; 3 mm diameter) glued on the goggles (figure 1(d)) using seven Qualisys motion capture cameras (Oqus 7 plus; 1000 Hz; 3 MP; Gothenburg, Sweden). These cameras were also used to determine the stroke plane angle, $\theta = 26^\circ$, and stroke amplitude of the bird at the middle of the 1 m flight. For this, we used retro-reflective tape (3M™ Scotchlite™ 7610 Reflective Tape) to mark and track the tips of the primary feathers at the leading edge of the right wing for two flights without flow recordings. Gaps in the tracking data were filled with a third-order polynomial using Qualisys Track Manager (QTM 2.11) software.

2.4. Still air background noise and filtering

We determined the background velocity and vorticity in the still air setup by analyzing ten consecutive velocity fields, from the same flight, recorded well before the bird flew through the laser sheet. The still air conditions were measured for flights 1–3 and decomposed in three orthogonal components (figure 1(b)) for all three flights; the streamwise velocity (-0.02 ± 0.09 ; -0.06 ± 0.14 ; $-0.04 \pm 0.10 \text{ m s}^{-1}$), the lateral velocity (0.03 ± 0.09 ; 0.05 ± 0.12 ; $0.06 \pm 0.10 \text{ m s}^{-1}$), and the vertical velocity (0.05 ± 0.04 ; 0.05 ± 0.14 ; $0.03 \pm 0.04 \text{ m s}^{-1}$) are very low compared to the body velocity of the bird (1.75 ; 1.50 ; 1.75 m s^{-1}) and the wingtip velocity ($\sim 13 \text{ m s}^{-1}$). The mean calculated background vorticity (-0.13 ± 6.43 ; 0.04 ± 8.00 ; $-.38 \pm 7.19 \text{ s}^{-1}$) during flights 1–3 is three orders of magnitude lower than the vorticity calculated in the tip vortex region. When we filtered vorticity we used a cut-off value of 23.8, 22.3, and 24.3 s^{-1} for flights 1, 2, and 3, respectively. The exception was the case when we implemented the Gaussian tail correction following Spedding *et al* (2003) and copied their use of a cut-off filter at 20% of the maximum vorticity of each vortex.

2.5. Three common models to calculate aerodynamic lift

We tested and contrasted the ability of three aerodynamic models: the Kutta–Joukowski theorem, KJT, the vortex ring model, VRM, and the actuator disk

model, ADM, to predict the lift generated by the bird as it passed through the laser sheet. The calculated average and instantaneous weight support based on these models varies across the literature and depends on the flight speed of the flying animal, the distance between the laser sheet and the flying animal, the animal species and the model parameters used (figure 2). Our calculations were based on the velocity and vorticity field measured at approximately mid-downstroke for all three flights. We subsequently permuted all model parameters used in the literature to determine how different choices influence the predicted lift.

First, we calculated the lift based on the Kutta–Joukowski theorem, KJT (e.g. Spedding *et al* 2003),

$$L_{\text{KJ}}(t) = \rho U \Gamma(t) b_w(t) \quad (1)$$

in which the lift, L_{KJ} , is a function of time, t , and depends on the air density, $\rho = 1.19 \text{ kg m}^{-3}$, the bird's body velocity, U , the quasi-steady variation of circulation in the wingtip vortex, $\Gamma(t)$, and the span of the wake, $b_w(t)$. The KJT ignores the interaction of body and wingtip vortices, as well as any 'added mass' effects due to flow acceleration. This simple equation was originally derived to predict the lift generated by wings flying at constant velocity based on the wake in a theoretical plane located infinitely far downstream, known as the 'Trefftz plane' (Drela 2014). In this plane, the vorticity sheet formed by the wing has rolled up into simple tip vortices. Trefftz plane integration thus greatly simplifies the calculation of lift, as explained in further detail in (Drela 2014). However, to what degree this theory applies to animal flight is unclear.

In wind tunnel studies, the flight speed U is usually replaced with the wind tunnel speed, U_∞ , (Hedenström *et al* 2006a, Henningsson *et al* 2008, Henningsson *et al* 2011, Muijres *et al* 2012b, Henningsson *et al* 2014, Henningsson *et al* 2015) or the wind speed combined with the flight velocity of the animal's body (Hubel *et al* 2009). However, the flapping motion of the wings creates additional velocity components during the downstroke that might exceed the forward velocity of the bird. An effective velocity that integrates the motion of the wings may be a better approximation for the velocity of the lifting surfaces, and can thus lead to more accurate estimates of lift. An average effective wing speed can be estimated as $U_{\text{eff}} = U_\infty \sqrt{(2St)^2 + 1}$ (Lentink and Gerritsma 2003), where the Strouhal number based on the tip-to-tip amplitude is $St = \phi Rf/U$. This more precise wing velocity estimate is thus a function of both the body speed and the Strouhal number of the flapping wing. This velocity correction was applied by Muijres *et al* (Muijres *et al* 2011a) as $U_{\text{eff}} = U_\infty \sqrt{St^2 + 1}$ for calculating the lift coefficient of a bat. Alternatively, Muijres *et al* (2008) and Muijres *et al* (2012a) integrated an effective velocity into the Kutta–Joukowski theorem using the average speed of the wing during the downstroke ($U_{\text{eff}} = |\{\bar{u} + U_\infty, \bar{w}\}|$, where \bar{u} and \bar{w} are the

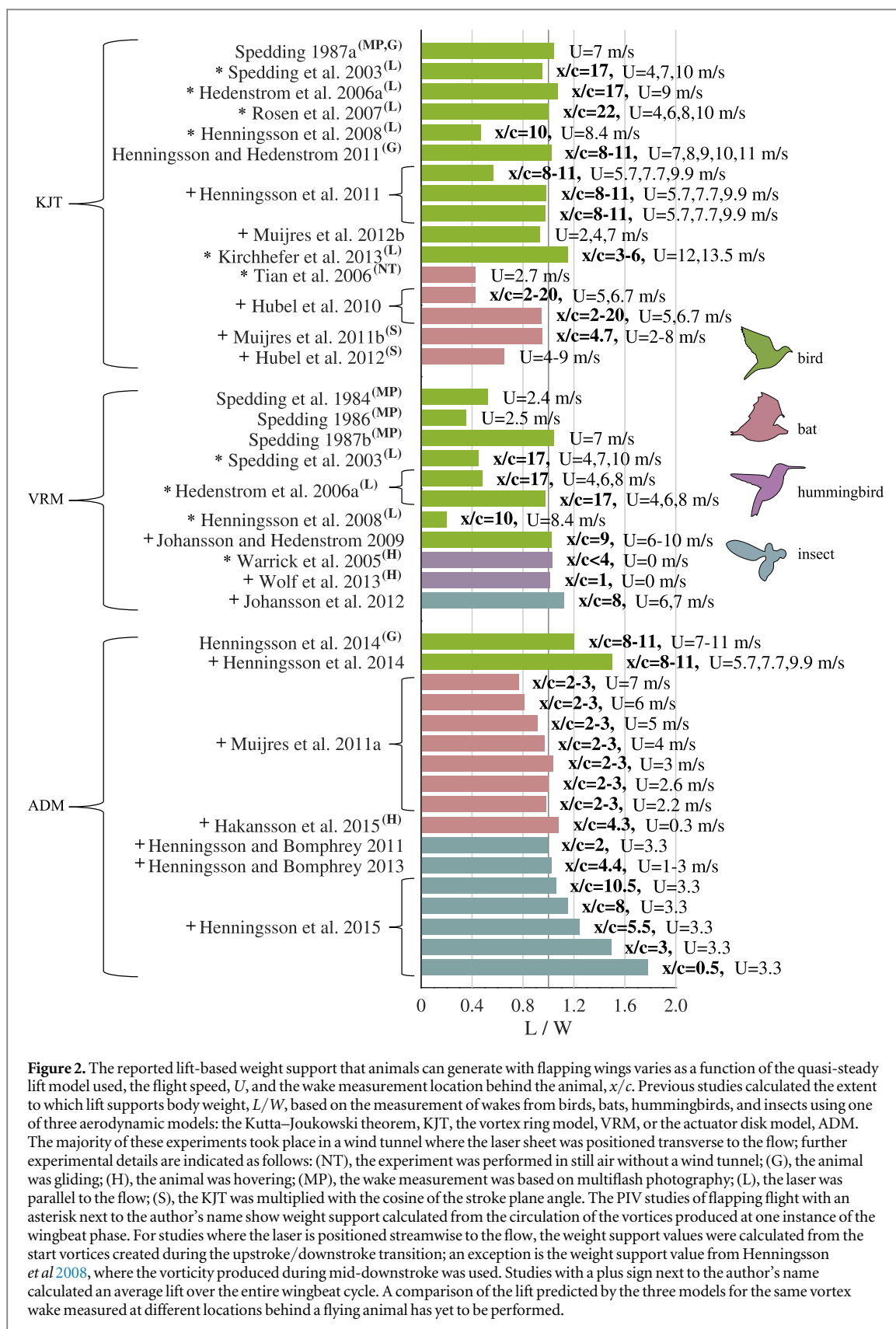


Figure 2. The reported lift-based weight support that animals can generate with flapping wings varies as a function of the quasi-steady lift model used, the flight speed, U , and the wake measurement location behind the animal, x/c . Previous studies calculated the extent to which lift supports body weight, L/W , based on the measurement of wakes from birds, bats, hummingbirds, and insects using one of three aerodynamic models: the Kutta–Joukowski theorem, KJT, the vortex ring model, VRM, or the actuator disk model, ADM. The majority of these experiments took place in a wind tunnel where the laser sheet was positioned transverse to the flow; further experimental details are indicated as follows: (NT), the experiment was performed in still air without a wind tunnel; (G), the animal was gliding; (H), the animal was hovering; (MP), the wake measurement was based on multiflash photography; (L), the laser was parallel to the flow; (S), the KJT was multiplied with the cosine of the stroke plane angle. The PIV studies of flapping flight with an asterisk next to the author’s name show weight support calculated from the circulation of the vortices produced at one instance of the wingbeat phase. For studies where the laser is positioned streamwise to the flow, the weight support values were calculated from the start vortices created during the upstroke/downstroke transition; an exception is the weight support value from Henningsson et al 2008, where the vorticity produced during mid-downstroke was used. Studies with a plus sign next to the author’s name calculated an average lift over the entire wingbeat cycle. A comparison of the lift predicted by the three models for the same vortex wake measured at different locations behind a flying animal has yet to be performed.

average horizontal and vertical velocities of the flapping wing, respectively). There is no consensus on what the best velocity correction is.

Some studies assume that equation (1) gives the combined lift and thrust produced by the vortex structures. To obtain the lift, L_{KJ} is multiplied by cosine of

the stroke plane angle, $\theta = 26^\circ$, which decreases the force calculated with equation (1) (Henningsson et al 2011, Muijres et al 2011b, Hubel et al 2012). Others assume that equation (1) gives the vertical lift and leave equation (1) as is (Spedding et al 2003, Tian et al 2006, Hedenström et al 2006a, Rosén et al 2007,

Henningsson *et al* 2008, Hubel *et al* 2010, Henningsson and Hedenström 2011, Muijres *et al* 2012b, Kirchhefer *et al* 2013). To compare results in this study, both assumptions were used to estimate lift, that is, we calculated lift both directly from equation (1) and from multiplying equation (1) by $\cos(\theta)$.

Second, we calculated the lift based on the vortex ring model, VRM (e.g. Spedding *et al* 2003),

$$L_{VR} = \frac{1}{T}I_z = \frac{1}{T}\rho\Gamma A_p \quad (2)$$

in which the lift, L_{VR} , is a function of the vertical impulse, I_z , of the vortex ring produced by the bird during the downstroke and the amount of time it takes to produce that impulse, T . I_z is a function of ρ , the vortex ring circulation, Γ , and the projected area, A_p , of the vortex ring onto a horizontal plane. Here, $A_p = \pi b_w(t)\lambda \cos\theta/4$ where $\lambda = 0.16$ m is the total length of the vortex ring (which we assumed to be approximately the distance traveled by the wingtips during the downstroke), and $\theta = 26^\circ$ is the stroke plane angle (figure 1(b)). This equation describes the wake as a discrete shedding of vortex rings during each downstroke and assumes an inactive upstroke, which is reasonable for our slow flying parrotlet (Lentink *et al* 2015). The predicted lift based on the vortex ring thus represents an average value for the entire downstroke. The vortex ring model corresponds to the wakes visualized in slow forward flights of small passerines, pigeons, and jackdaws (Kokshaysky 1979, Spedding *et al* 1984, Spedding 1986, Spedding *et al* 2003). The formation of these rings and the buildup of their associated circulation is best understood for engineered vortex ring generators (Gharib *et al* 1998, Rosenfeld *et al* 2009).

Third, we calculated the lift based on the actuator disk model, ADM (e.g. Håkansson *et al* 2015),

$$L_{AD}(t) = 2\dot{m}(t)w(t) = 2\rho A_d(t)\overline{w^2}(t) \quad (3)$$

in which the lift, L_{AD} , is a function of the mass flux through the vortex ring produced during the downstroke, $\dot{m}(t)$, and the spanwise-average of the squared downwash of the vortex ring $\overline{w^2}(t)$. The mass flux is a function of ρ , $w(t)$, and the vortex ring area, $A_d(t) = \pi b_w(t)\lambda/4$. The predicted lift represents the mid-downstroke weight support, because we calculate the lift using the mid-downstroke downwash. In this equation, the streamwise component of the induced velocity vector is ignored. In a series of studies, the downwash was usually calculated along a line between the vortex and the center of the body (Muijres *et al* 2011a, Johansson *et al* 2012, Muijres *et al* 2012b). In this study, the downwash was obtained in a similar fashion, by averaging the velocity values along a horizontal line between the wingtip vortex and the median plane of the bird's body.

In bird wake studies in wind tunnels, it is generally observed that the wake contracts as it is advected to the laser sheet. Thus, the span of the wake, or the distance between the left and right wingtip vortices at the laser sheet, is usually used as the parameter in the lift

equations (Henningsson *et al* 2011, Muijres *et al* 2012b, Henningsson *et al* 2014). Others use the wingspan of the bird when the wake is generated (Henningsson *et al* 2008, Hubel *et al* 2010). In the study of a swift's wake, Henningsson *et al* underestimated the lift by 50% when the wake span was used, but obtained a lift closer to the weight of the bird when the wingspan of the bird was used (Henningsson *et al* 2011). In contrast, wake contraction was minimal and did not have much influence on the lift calculations of a desert locust (Henningsson and Bomphrey 2011). In another study, care was taken to position a hawkmoth in the wind tunnel such that the distance between the hawkmoth and the laser sheet was far enough for the wake to contract and for vorticity to roll up into the tip vortices, but not so far that the wake became twisted or largely deformed (Henningsson and Bomphrey 2013). To compare results in our study, both definitions of span based on the wing and the wake were used to estimate lift.

2.6. Reference vertical force measurement for midstroke

To contrast the lift calculation based on the three aerodynamic models, we compared these predictions with direct measurements of vertical force during the mid-downstroke in freely flying Pacific parrotlets ($N = 4$; $n = 3$) using an aerodynamic force platform (AFP). This new method to measure aerodynamic force directly *in vivo* is further explained in Lentink *et al* 2015. The flight volume used for these force recordings is 1.0 m long, 0.9 m high, and 0.6 m wide, and the two perches were located 0.75 m apart. The average weight support measured in the AFP was $101\% \pm 3\%$ of bodyweight ($N = 4$, $n = 5$), which is close to the 100% expected based on conservation of momentum for a flight that starts and ends at rest. The corresponding instantaneous vertical force measured during mid-downstroke with the AFP was 2.40 ± 0.25 (mean \pm std, across 12 flights, $N = 4$, $n = 3$) normalized by bodyweight. For this average we selected the wingbeat from each flight that best corresponded with the wingbeat kinematics recorded in the laser sheet of the present study.

3. Results

For all three flights we found that the dynamics of the right wingtip vortex goes through three distinct stages as the vortex advects downward in the laser sheet and finally breaks up. In the first stage the wingtip vortex is created and rolls up with a relatively constant diameter. In the second stage the diameter of the vortex starts to increase just before it breaks up. In the third stage the vortex experiences a rapid expansion and chaotic breakup into multiple vortices that interact. For all three flights, we ignored the vortex that was visualized prior to the wingstroke analyzed

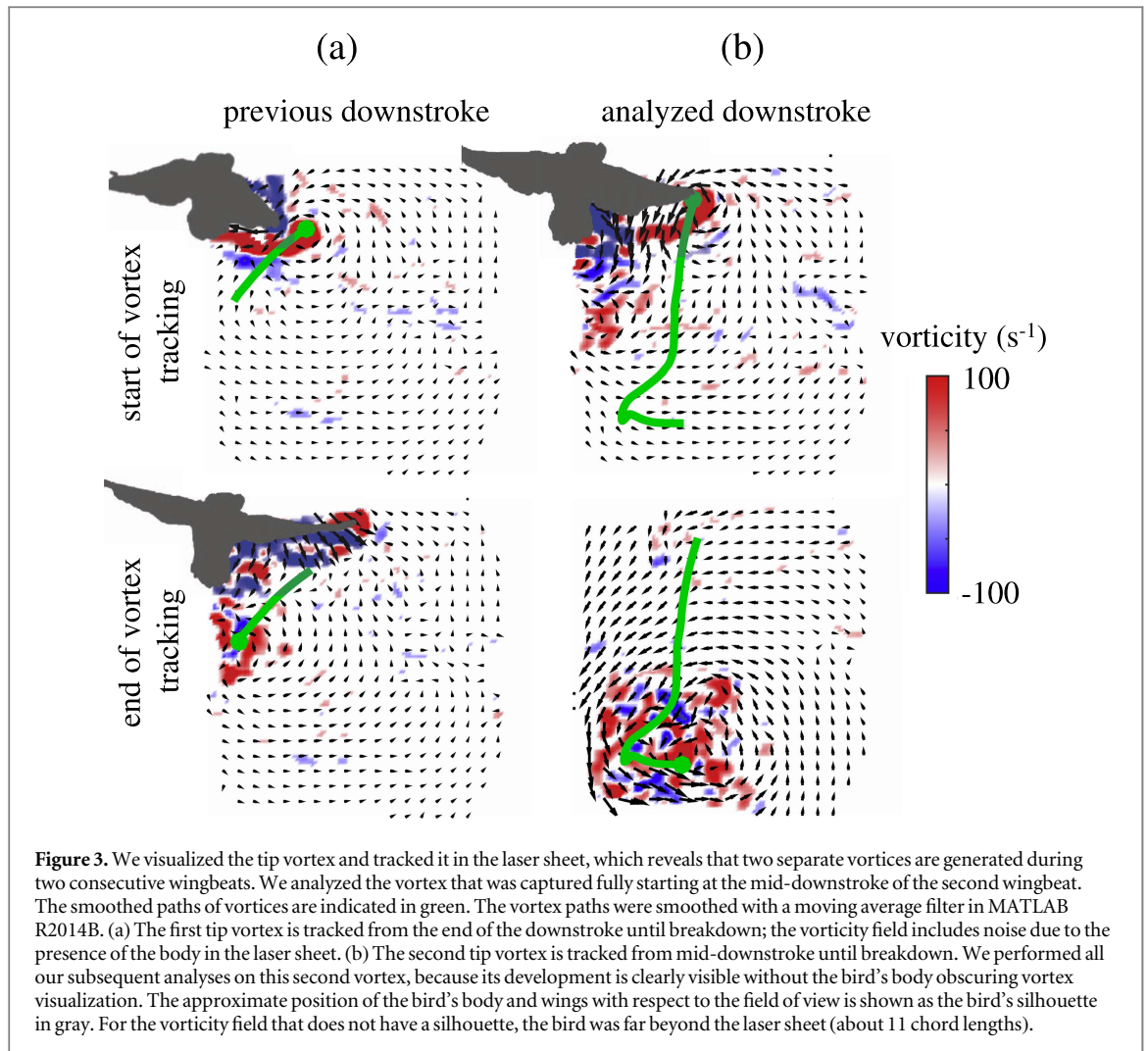
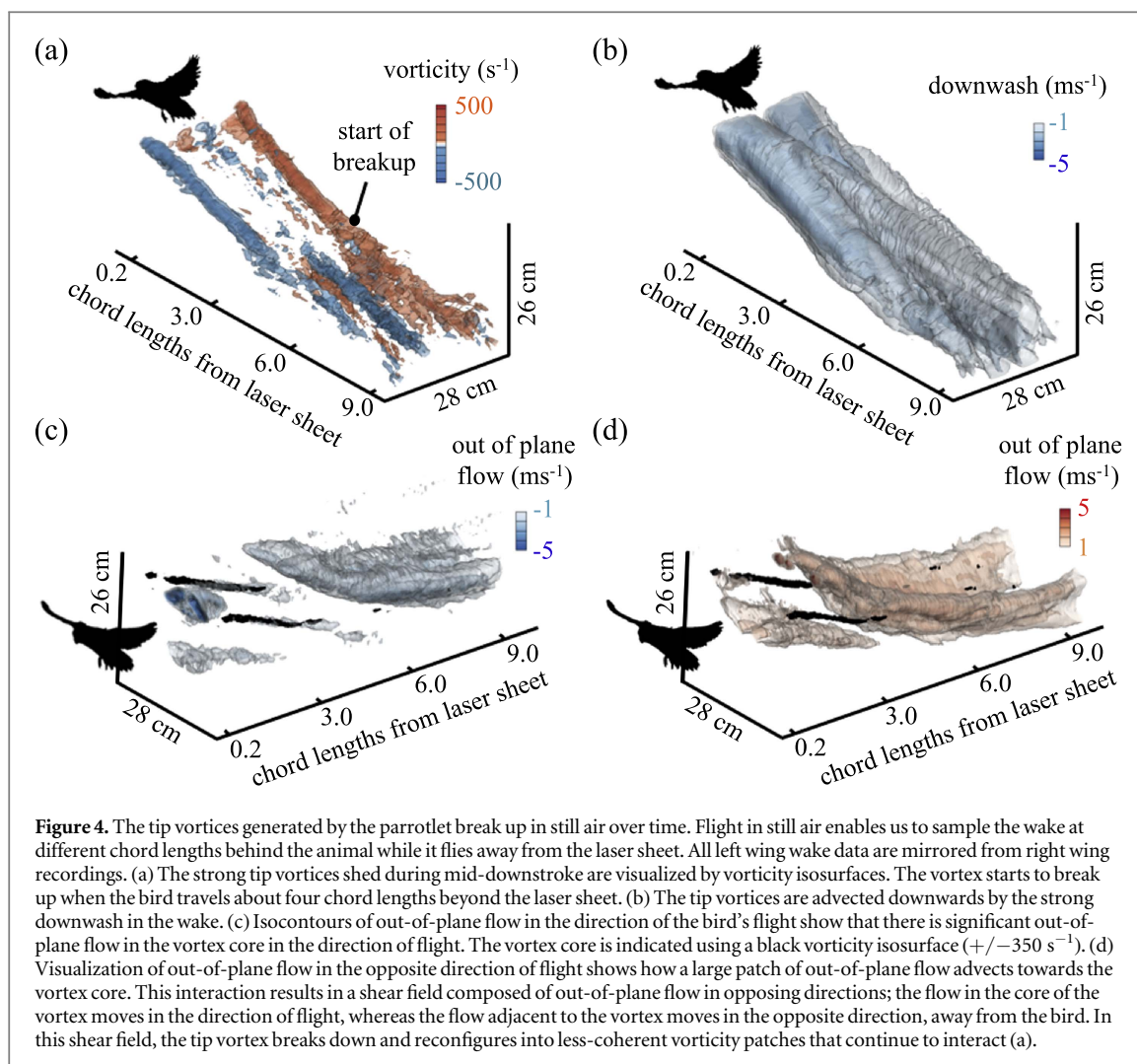


(figure 3(a)) and focused on the tip vortex generated while the wing fully passed through the laser sheet approximately mid-downstroke (figure 3(b)). This enabled us to track the development of the tip vortex during the quasi-steady phase of the wingbeat (Lentink and Dickinson 2009), for which the three models are expected to be most applicable. The center of the wingtip vortex was tracked by calculating the maximum vorticity in a square area around the vortex for each frame. Tracking was started when the bird's wing no longer interfered with the vortex. The tracked tip vortices had the longest lifetimes and broke up at similar times after the vortex was first visualized in the laser sheet. The tip vortices broke up after 0.08–0.12 s, which is equivalent to about two or three wingbeat periods and corresponds to about 4.5–6 chord lengths travel of the bird beyond the laser sheet (figure 4(a)). Most published wind tunnel studies present wakes that fall within or exceed this range in chord lengths behind the animal (figure 2). Because the vortex circulation and the calculated weight support are similar for all three flights, we present the flow fields and calculations for the third flight here (figures 3–6) and present results for flights 1 and 2 in the online supplementary materials (figures S2–S8).

The flow fields obtained in still air include the streamwise, transverse and vertical velocity fields and the vorticity field in a plane behind the bird as a function of time (figures 3(b); 4; 5(a)). This plane, which better approximates a Trefftz plane the further the bird flies beyond the laser sheet, represents a single phase in the wingbeat. In contrast, wake recordings at a fixed x/c position (measured in chord lengths) behind an animal in a wind tunnel continuously sample the wake associated with the ongoing wingbeat cycle. As a result, wind tunnel recordings sample the entire wingbeat at a more or less fixed x/c position of the wake plane behind the animal, which limits the ability to study how the vortex wake develops downstream. Wind tunnel studies can thus estimate the quasi-steady lift throughout the entire wingbeat cycle, whereas still air studies can estimate the quasi-steady force only for the associated stroke phase when the bird moves its wing through the laser sheet. If the wake is indeed 'frozen' during its advection downstream in a wind tunnel, or its development in still air, the phase-locked lift estimate should remain constant for all x/c .

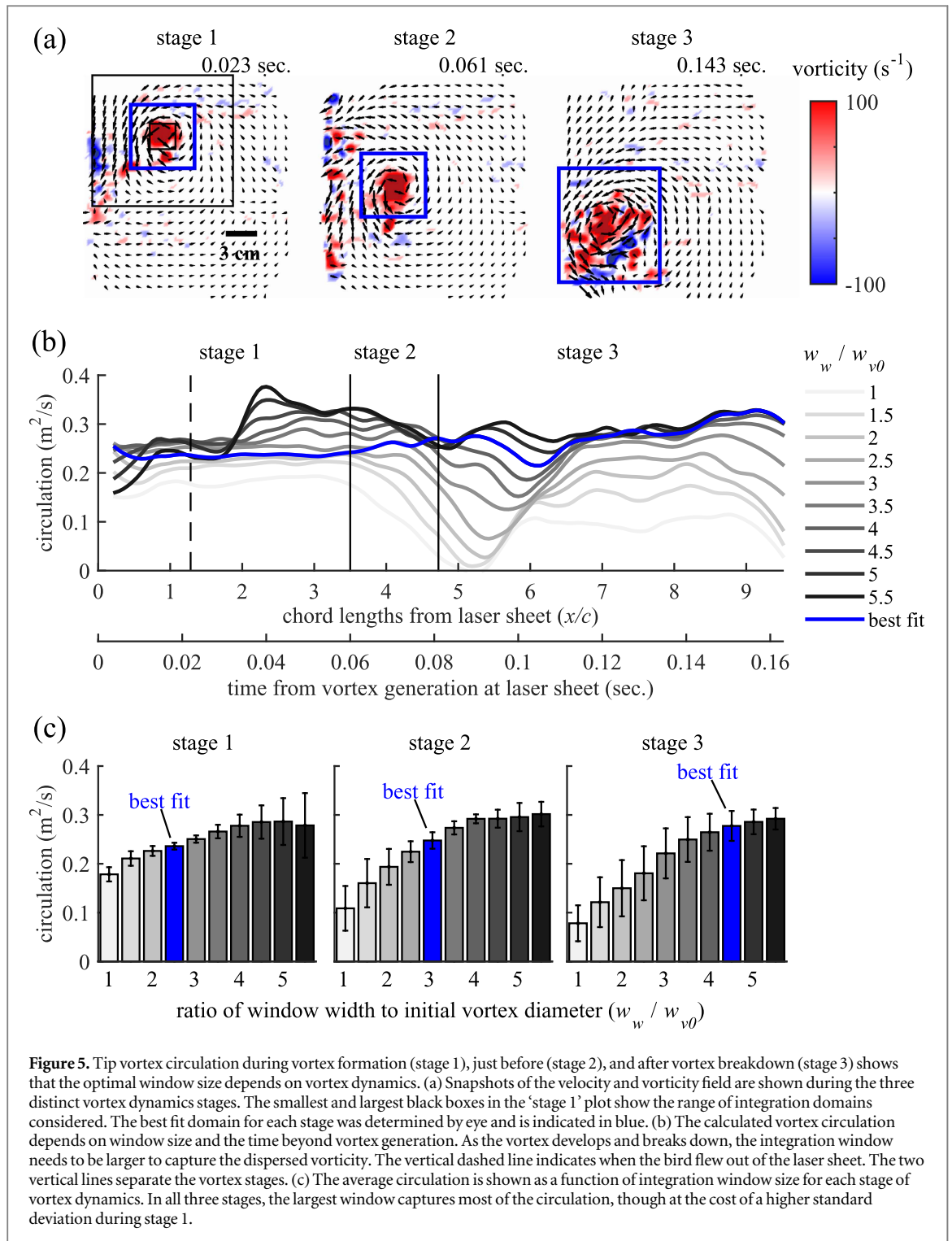
To evaluate how constant the phase-locked vortex strength is in still air, we determined how the circulation of the tip vortex developed over time. The



instantaneous circulation of the vortex was obtained by integrating its vorticity within a window (figure 5(a)). The center of the window was determined by the location of peak vortex vorticity. Because the preferred window size varies in the literature, we determined how size influences the calculation of circulation (figures 5(b), (c)). We also selected an optimal window size by eye for each vortex evolution stage, which took into account the size of the tracked vortex and nearby vortex structures. For the first two stages, a window size of about twice the diameter of the wingtip vortex captured the circulation with minimal variation over time. As the vortex broke up, the size of the window was increased to take into account the increase in area over which the remaining vortical structures evolved. Determination of the optimal window size became cumbersome and less reliable as soon as the vortex broke up during stage 3. The 'optimized' window size was carefully determined by eye to ensure all vortex structures that originated from the burst vortex were included. Procedures guided by eye do not have algorithmic repeatability, which is why we compared results with constant window sizes. This was essential, because we do not know of an algorithm (e.g. Chakraborty et al 2005, Berson et al 2009, Jones

et al 2011, Jones et al 2016) that can objectively identify the representative center of a burst vortex and all its associated vorticity automatically in a complex wake. This is probably why the maximum vorticity was tracked in previous studies of complex vortex wakes of birds and other flying animals (e.g. Spedding et al 2003, Johansson and Hedenström 2009).

We calculated the lift predicted by all three models for each vortex dynamics stage as a function of the bird's distance from the laser sheet in chord lengths, x/c (figure 6(a)). We compared these 'phase-locked' lift predictions for the mid-downstroke with instantaneous vertical force recordings obtained with an AFP (figure 6). The lift to weight ratio, L/W , measured with the AFP was 2.40 ± 0.25 during mid-downstroke (figure 6(a)). During the first vortex dynamics stage, L/W is 0.31 for the Kutta–Joukowski theorem, 1.14 for the vortex ring model, and 2.95 for the actuator disk model based on wake span b_w (figure 6(a)). The values for KJT could be increased by better estimating the wingtip speed (Lentink and Gerritsma 2003, Muijres et al 2011a) mid-downstroke when the vortex is first recorded. The predicted lift would increase by a factor of 8.6 to about 2.67 (wing velocity $R\phi\pi f$, stroke plane angle $\theta = 26^\circ$, horizontal body velocity



$U \approx 1.7 \text{ m s}^{-1}$; wing tip speed $\sim 13 \text{ m s}^{-1}$). For both the Kutta–Joukowski theorem and vortex ring model, the weight support stays relatively constant from the time the vortex is formed to when it exits the field of view after breakdown (stages 1–3), as it should according to the assumptions of a quasi-steady analysis. For the actuator disk model, however, we found that lift decreases to almost zero when the vortex breaks up. Similar vortex dynamics and values of weight support were found for the other two flights (see online supplementary figures S7 and S8). The differences between

the KJT and VRM versus ADM in their ability to predict constant lift for a specific wingbeat phase were independent of the permutations of different model parameters (figure 6) and similar for all three flights (figure 7).

Finally, to determine to what extent vorticity field filtering might affect the ability of the vortex based models (KJT and VRM) to predict constant lift, we contrasted three common approaches. The vorticity of the main vortex structures is generally found in one of three ways: (1) from the entire field of view assuming

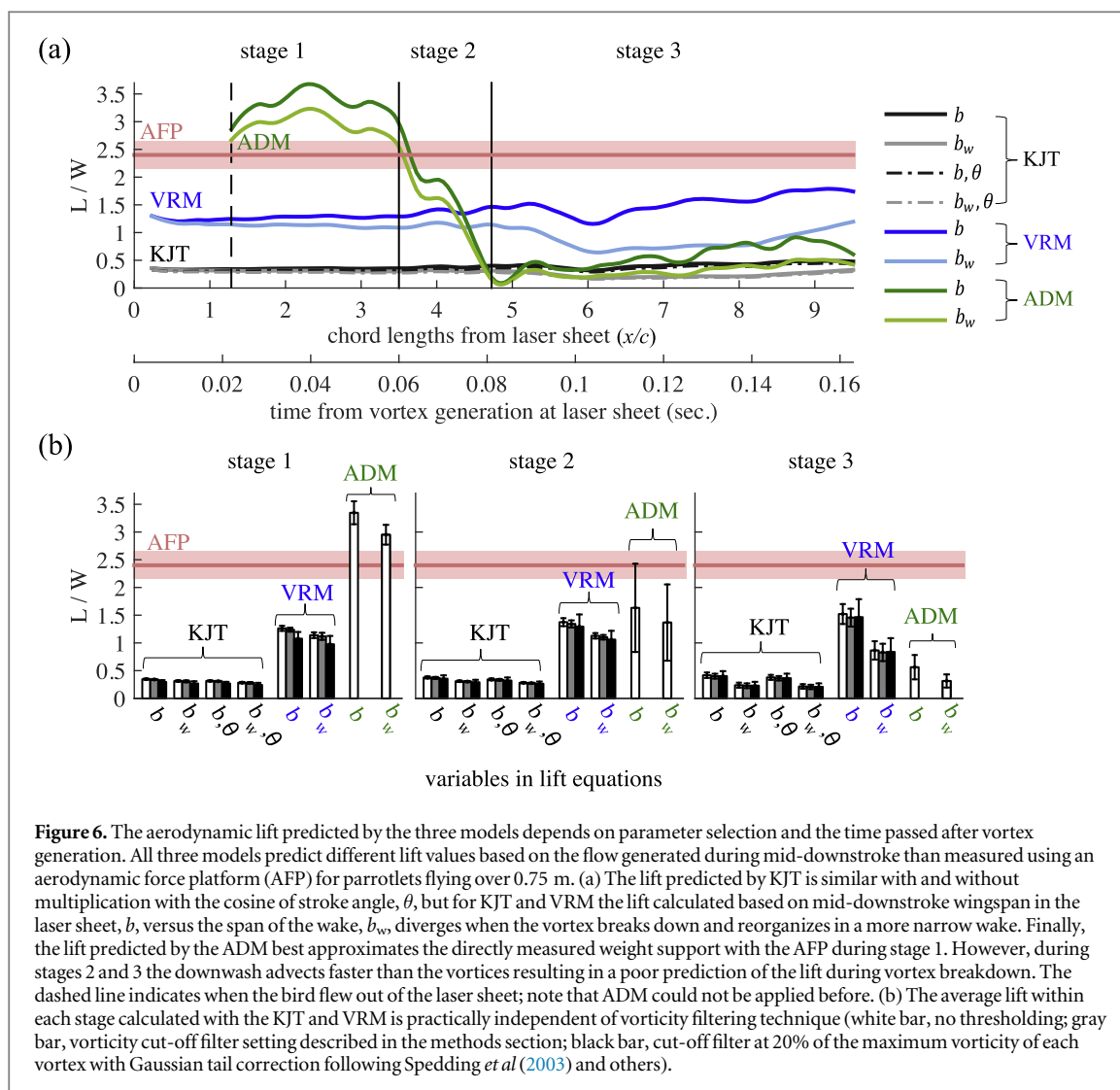


Figure 6. The aerodynamic lift predicted by the three models depends on parameter selection and the time passed after vortex generation. All three models predict different lift values based on the flow generated during mid-downstroke than measured using an aerodynamic force platform (AFP) for parrotlets flying over 0.75 m. (a) The lift predicted by KJT is similar with and without multiplication by the cosine of stroke angle, θ , but for KJT and VRM the lift calculated based on mid-downstroke wingspan in the laser sheet, b , versus the span of the wake, b_w , diverges when the vortex breaks down and reorganizes in a more narrow wake. Finally, the lift predicted by the ADM best approximates the directly measured weight support with the AFP during stage 1. However, during stages 2 and 3 the downwash advects faster than the vortices resulting in a poor prediction of the lift during vortex breakdown. The dashed line indicates when the bird flew out of the laser sheet; note that ADM could not be applied before. (b) The average lift within each stage calculated with the KJT and VRM is practically independent of vorticity filtering technique (white bar, no thresholding; gray bar, vorticity cut-off filter setting described in the methods section; black bar, cut-off filter at 20% of the maximum vorticity of each vortex with Gaussian tail correction following Spedding *et al* (2003) and others).

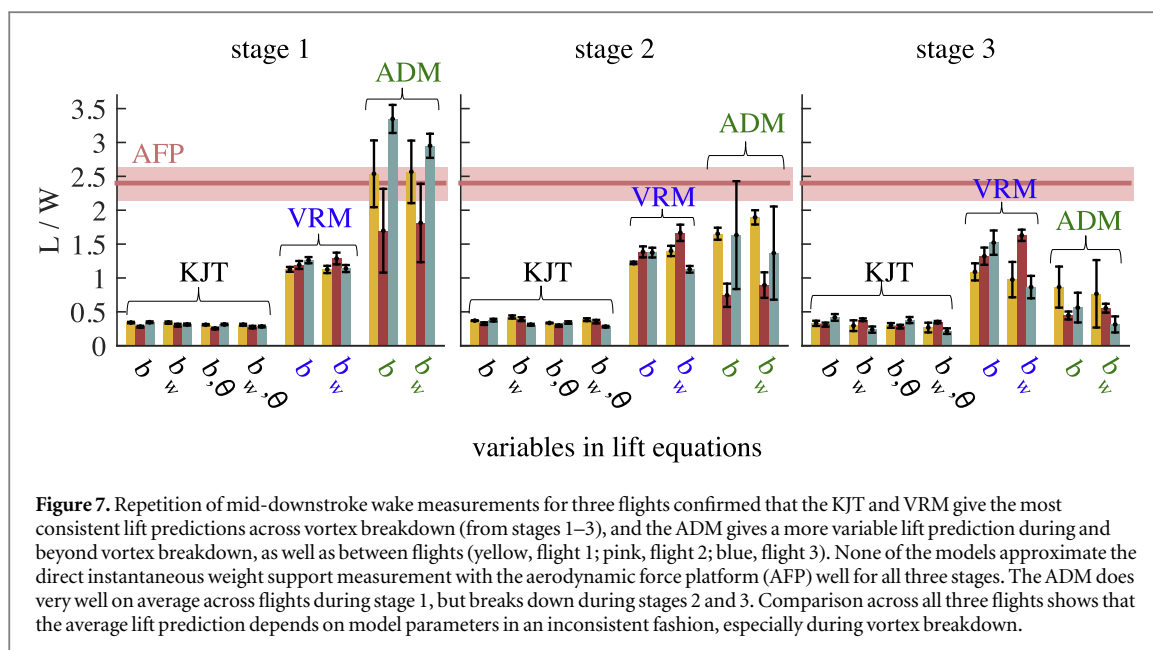


Figure 7. Repetition of mid-downstroke wake measurements for three flights confirmed that the KJT and VRM give the most consistent lift predictions across vortex breakdown (from stages 1–3), and the ADM gives a more variable lift prediction during and beyond vortex breakdown, as well as between flights (yellow, flight 1; pink, flight 2; blue, flight 3). None of the models approximate the direct instantaneous weight support measurement with the aerodynamic force platform (AFP) well for all three stages. The ADM does very well on average across flights during stage 1, but breaks down during stages 2 and 3. Comparison across all three flights shows that the average lift prediction depends on model parameters in an inconsistent fashion, especially during vortex breakdown.

that the positive and negative vorticity due to background noise and turbulence cancel (Hubel *et al* 2009); (2) by integrating the vorticity that rises above a

threshold value and adding back an estimate for the neglected vorticity; here, the cut-off filter is at 20% of the maximum vorticity of each vortex with Gaussian

tail correction (Spedding *et al* 2003, Hedenström *et al* 2006a, Hedenström *et al* 2006b, Hedenström *et al* 2009, Muijres *et al* 2011b, Wolf *et al* 2013); or (3) by applying a lower threshold to erase the background vorticity without correction (Hubel *et al* 2010). Our results show that the average L/W varies only slightly among the different noise mitigation strategies (figure 6(b)). Because the results are similar, we assumed that positive and negative background vorticity would cancel and did not filter vorticity in our integration area (figures 6(a), 7).

4. Discussion

We found consistent evidence for vortex breakdown in the wake of the parrotlet during all recorded flights ($n = 3$, figure 4; supplementary figures S3 and S4) at an advance ratio of about $J = 0.2$. We also found vortex breakdown during our earlier pilot recordings including those with another individual (making $N = 2$ for this observation, supplementary figure S1). Vortex breakdown occurs in a complex shear field buildup by streamwise core flow in the vortex and opposite streamwise flow patches around the tip vortex (figures 4(c), (d); S3(c), (d); S4(c), (d)). In all cases considered, the vortex broke down two to three wingbeats after being shed (figures 4(a); S3(a); S4(a)). Our recordings thus suggest that idealized vortex wake representations will probably only hold up to a maximum of about three staggered vortex rings. This quick breakdown implies that the common vortex ring model of animal flight is only applicable in the near wake of slowly flying birds. Vortex breakdown also violates the ‘frozen turbulence’ hypothesis that is commonly assumed to hold for animal wakes (e.g. Johansson and Hedenström 2009, Henningsson *et al* 2011), because the spatial and temporal velocity correlations are no longer similar when coherent vortices break down (Pope 2000).

Our side-by-side comparison of the three lift models, for the same flow fields, shows that vortex breakdown renders these lift calculations inconsistent. This inconsistency is found across the various permutations of model parameters (figure 6(a)) and flights (figure 7). The effect of a stroke plane angle of 26° on predicted lift is minor, because the cosine is ~ 0.9 (figure 6(a)). In contrast, the effect of wake span development on KJT and VRM lift prediction is significant (figure 6(a); stages 2 and 3). During vortex breakdown the location of the vortex center becomes more ambiguous, because the vortex reorganizes into multiple vortex patches (figures 3–5). This complicates the calculation of the wake span, which either decreases or increases across flights (figure 6(a); supplementary figures S7 and 8). The various inconsistencies due to vortex dynamics are much reduced by averaging the

lift in each of the three stages (figure 6(b)), which results in more constant lift prediction across vortex dynamics stages 1–3, as expected under the quasi-steady assumption. This constancy of vortex circulation is similar to findings for bats (Johansson *et al* 2008, Hubel *et al* 2009, Hubel *et al* 2010). Whereas stage-averaging significantly improves the stability of the KJT and VRM lift prediction, the very reasonable ADM prediction during stage 1 is particularly sensitive and fails during and after vortex breakdown (stages 2 and 3), regardless of stage-averaging. These findings for KJT and VRM are independent of vorticity field filtering (figure 6(b)) and circulation integration window size, which further shows that these calculations are particularly robust (Johansson *et al* 2008, Hubel *et al* 2009, Hubel *et al* 2010).

All three lift models predict different levels of weight support during mid-downstroke, ranging from only 13% of the directly measured vertical force for KJT without the velocity correction, to 48% for VRM, and up to 123% for ADM before vortex breakdown initiates (stage 1, flight 3). Whereas the KJT and ADM provide instantaneous lift estimates, the VRM gives a downstroke-averaged value for which the instantaneous AFP recording comparison is less relevant. However, given that slowly flying parrotlets generate downstroke-averaged lift close to two times body-weight to make up for the ‘inactive’ upstroke (Lentink *et al* 2015), we still find that the VRM underpredicts lift by about a factor of two. The large weight support underestimation of the uncorrected KJT mid-downstroke is not entirely surprising. The KJT is derived for steady fixed wings, which are not representative of active animal flight in which the wings are flapped and have a higher effective velocity. A similar wake study of bats with a similar body mass, flying at speeds between 2 and 3 m s^{-1} in still air, also found low L/W values of about 0.43 using the KJT based on forward flight speed (Tian *et al* 2006). Correcting KJT by using the effective wing speed throughout the wingbeat yields a lift estimate much closer ($\sim 110\%$) to the value measured with the AFP. Based on the effectiveness of the velocity correction and the theoretical support by the work of Noca *et al* (1997) and others, the development of rigorously derived correction factors could make KJT more applicable. In contrast, the very reasonable initial ADM prediction during stage 1 consistently reduces to a value close to zero during (stage 2) and after vortex breakdown (stage 3) (figures 6, 7), which cannot be reconciled with a correction factor. In general, this discrepancy is likely to be even worse for other phases of the wingstroke, because quasi-steady models are expected to be most applicable mid-downstroke. The vertical force recorded with the aerodynamic force platform (AFP; figure 6) during mid-downstroke corresponds with earlier published AFP vertical force recordings for parrotlets (Lentink

et al 2015). These force recordings, which show how parrotlets generate weight support primarily during the downstroke, correspond with the large tip vortex that we find during the downstroke, but not during the upstroke.

Remarkably, our wake visualizations show that prior to vortex breakdown in stage 3, the flow is coherent and relatively simple during stages 1 and 2, for which ADM predicts lift best, and KJT needs a large correction factor. We found that the three models predict lift similarly across all three flights, and that ADM is consistently unreliable during vortex breakdown (figure 7). The limitations found in our analysis probably also apply to other variations of the ADM model (Bomphrey *et al* 2006, Henningsson and Bomphrey 2011, Henningsson and Bomphrey 2013, Henningsson *et al* 2015). The inaccuracy of the models is unlikely to be caused by added mass effects, because the dimensionless wake vortex ratio, W_a , that Dabiri (Dabiri 2005, Dabiri *et al* 2006) proposed for estimating the unsteadiness of vortex wakes generated by animals, is approximately 0.15 ($l_v \approx 0.03$ m, $U_v \approx 1.6$ m s⁻¹, $\Gamma \approx 0.23$ m² s⁻¹) for our parrotlet, which is below the critical value of 0.42. However, all three models tested here are expected to underperform to some extent at an advance ratio of $J = 0.2$, because the flow is more complex and unsteady than during fast forward flight, where quasi-steady models provide a better approximation (Lentink and Dickinson 2009). The exclusion of unsteady effects in the calculation of lift may thus help explain lift underestimation in animal flight (figure 2). Reconciling these constraints is not straightforward, because all three models seem to be impacted differently at a low advance ratio, resulting in different levels of lift prediction (figure 7). The imprecise calculation of lift can be further explained by the omission of stress and pressure terms, and the omission of the frontal, side, bottom and top plane contributions to the control volume formulation that underpins the three quasi-steady models. Our comparison of predicted *versus* measured mid-downstroke force generation confirms earlier concerns about the limited applicability of quasi-steady lift models such as KJT to flapping wings (Minotti 2011, Wang *et al* 2013, Liu *et al* 2015, Wang *et al* 2015)—and animal locomotion in general (Dabiri 2005). Our comparison of aerodynamic forces recorded directly with an AFP (Lentink *et al* 2015) with quasi-steady lift predictions based on wake measurements is the first *in vivo* validation of these models in animal flight. The comparison suggests that quasi-steady lift models have a limited applicability to animals flying at relatively low advance ratios. A future AFP setup developed for wind tunnel measurements at higher speeds (Lentink *et al* 2015) could further validate the accuracy of the three quasi-steady models for higher advance ratios.

5. Conclusions

This study compares the predictive strength of the three most popular lift models for calculating bodyweight support as a function of the distance between the laser sheet and a slowly flying bird. Although computational and robot-based flapping wing studies have already shown that quasi-steady lift models perform poorly, these models are still widely used in animal flight studies. Our study surveys and confirms the limitations for slowly flying animals. The models are sensitive to input parameters, and this must be taken into account when comparing the aerodynamic performance of animals across studies. To enable such meta studies, it would greatly help if future animal wake studies report results obtained for all three models and their various parameter choices. These studies should also more explicitly test the assumptions needed to apply these models. In particular, our study suggests that the wake symmetry assumption and frozen turbulence hypothesis used in most previous studies are not generally valid across animal flight. Our study shows that there is a need to improve the predictive strength of aerodynamic lift models based on measured animal wakes, in particular for lower advance ratios, and possibly higher ones as well. Whereas previous studies created vortex wake cartoons that helped convey the general topology of the vortex wake to a broad audience, these models may be overly simplified. For our slow flying parrotlet, we see additional complexity in the form of vortex breakdown. These complex vortex dynamics have received little attention during previous studies and are worthy of further study across different flight conditions and species. Such comparative studies are particularly valuable for identifying the aerodynamic principles that vertebrates use to generate lift, which are still poorly understood in general (Chin and Lentink 2016), despite their potential to improve the design of bioinspired wings.

Acknowledgments

This project is supported by Office of Naval Research (ONR) Multidisciplinary University Research Initiative (MURI) grant N00014-09-1051, the KACST Center of Excellence for Aeronautics and Astronautics at Stanford, a NDSEG fellowship to EG and a Stanford Graduate Fellowship to DDC. We would like to thank Matthew Molina for his support. We thank Florian T Muijres for sharing his laser goggle procedure and design as a starting point for our study and members of the Lentink lab for support.

References

- Ben-Gida H, Kirchhefer A, Taylor A J, Bezner-Kerr W, Guglielmo C G, Kopp G A and Gurka R 2013 Estimation of unsteady aerodynamics in the wake of a freely flying european starling (*Sturnus vulgaris*) *PLoS One* **8** e80086

- Berson A, Michard M and Blank-Benon P 2009 Vortex identification and tracking in unsteady flows *C. R. Mec.* **337** 61–7
- Bomphrey R J, Henningsson P, Michaelis D and Hollis D 2012 Tomographic particle image velocimetry of desert locust wakes: instantaneous volumes combine to reveal hidden vortex elements and rapid wake deformation *J. R. Soc. Interface* **9** 3378–86
- Bomphrey R J, Taylor G K, Lawson N J and Thomas A L R 2006 Digital particle image velocimetry measurements of the downwash distribution of a desert locust *Schistocerca gregaria* *J. R. Soc. Interface* **3** 311–7
- Chakraborty P, Balachandar S and Adrian R J 2005 On the relationships between local vortex identification schemes *J. Fluid Mech.* **535** 189–214
- Chin D D and Lentink D 2016 Flapping wing aerodynamics: from insects to vertebrates *J. Exp. Biol.* **219** 920–32
- Dabiri J O 2005 On the estimation of swimming and flying forces from wake measurements *J. Exp. Biol.* **208** 3519–32
- Dabiri J O, Colin S P and Costello J H 2006 Fast-swimming hydromedusae exploit velar kinematics to form an optimal vortex wake *J. Exp. Biol.* **209** 2025–33
- Drela M 2014 *Flight Vehicle Aerodynamics* (Cambridge, MA: MIT Press)
- Garrick I E 1936 Propulsion of a flapping and oscillating airfoil *NACA Report* 537
- Gemmell B J, Colin S P, Costello J H and Dabiri J O 2015 Suction-based propulsion as a basis for efficient animal swimming *Nat. Commun.* **6** 8790
- Gharib M, Rambod E and Shariff K 1998 A universal time scale for vortex ring formation *J. Fluid Mech.* **360** 121–40
- Gopalan H and Povitsky A 2010 Lift enhancement of flapping airfoils by generalized pitching motion *J. Aircr.* **47** 1884–97
- Håkansson J, Hedenström A, Winter Y and Johansson L C 2015 The wake of hovering flight in bats *J. R. Soc. Interface* **12** 20150357
- Hedenström A, Rosén M and Spedding G R 2006a Vortex wakes generated by robins *Erithacus rubecula* during free flight in a wind tunnel *J. R. Soc. Interface* **3** 263–76
- Hedenström A, van Griethuisen L, Rosén M and Spedding G R 2006b Vortex wakes of birds: recent developments using digital particle image velocimetry a wind tunnel *Anim. Biol.* **56** 535–49
- Hedenström A, Muijres F, von Busse R, Johansson L C, Winter Y and Spedding G R 2009 High-speed stereo DPIV measurement of wakes of two bat species flying freely in a wind tunnel *Exp. Fluids* **46** 923–32
- Henningsson P and Bomphrey R J 2011 Time-varying span efficiency through the wingbeat of desert locusts *J. R. Soc. Interface* **9** 1177–86
- Henningsson P and Bomphrey R J 2013 Span efficiency in hawkmoths *J. R. Soc. Interface* **10** 20130099
- Henningsson P and Hedenström A 2011 Aerodynamics of gliding flight in common swifts *J. Exp. Biol.* **214** 382–93
- Henningsson P, Hedenström A and Bomphrey R J 2014 Efficiency of lift production in flapping and gliding flight of swifts *PLoS One* **9** e90170
- Henningsson P, Michaelis D, Nakata T, Schanz D, Geisler R, Schroder A and Bomphrey R J 2015 The complex aerodynamic footprint of desert locusts revealed by large-volume tomographic particle image velocimetry *J. R. Soc. Interface* **12** 20150119
- Henningsson P, Muijres F T and Hedenström A 2011 Time-resolved vortex wake of a common swift flying over a range of flight speeds *J. R. Soc. Interface* **8** 807–16
- Henningsson P, Spedding G R and Hedenström A 2008 Vortex wake and flight kinematics of a swift in cruising flight in a wind tunnel *J. Exp. Biol.* **211** 717–30
- Horstmann J T, Henningsson P, Thomas A L R and Bomphrey R J 2014 Wake development behind paired wings with tip and root trailing vortices: consequences for animal flight *PLoS One* **9** e91040
- Hubel T Y, Hristov N I, Swartz S M and Breuer K S 2009 Time-resolved wake structure and kinematics of bat flight *Exp. Fluids* **46** 933–43
- Hubel T Y, Hristov N I, Swartz S M and Breuer K S 2012 Changes in kinematics and aerodynamics over a range of speeds in *Tadarida brasiliensis*, the Brazilian free-tailed bat *J. R. Soc. Interface* **9** 1120–30
- Hubel T Y, Riskin D K, Swartz S M and Breuer K S 2010 Wake structure and wing kinematics: the flight of the lesser dog-faced fruit bat, *Cynopterus brachyotis* *J. Exp. Biol.* **4** 3427–40
- Johansson L C and Hedenström A 2009 The vortex wake of blackcaps (*Sylvia atricapilla* L.) measured using high-speed digital particle image velocimetry (DPIV) *J. Exp. Biol.* **212** 3365–76
- Johansson L C, Engel S, Baird E, Dacke M, Muijres F T and Hedenström A 2012 Elytra boost lift, but reduce aerodynamic efficiency in flying beetles *J. R. Soc. Interface* **9** 2745–8
- Johansson L C, Wolf M, von Busse R, Winter Y, Spedding G R and Hedenström A 2008 The near and far wake of Pallas' long tongued bat (*Glossophaga soricina*) *J. Exp. Biol.* **211** 2909–18
- Jones A R, Medina A, Spooner H and Mulleners K 2016 Characterizing a burst leading-edge vortex on a rotating flat plate wing *Exp. Fluids* **57** 1–16
- Jones A R, Pitt Ford C W and Babinsky H 2011 Three-dimensional effects on sliding and waving wings *J. Aircr.* **48** 633–44
- Kirchhefer A J, Kopp G A and Gurka R 2013 The near wake of a freely flying European starling *Phys. Fluids* **25** 051902
- Kokshaysky N V 1979 Tracing the wake of a flying bird *Nature* **279** 329–51
- Lentink D and Dickinson M H 2009 Biofluiddynamic scaling of flapping, spinning and translating fins and wings *J. Exp. Biol.* **212** 2691–704
- Lentink D and Gerritsma M 2003 Influence of airfoil shape on performance in insect flight *Proc. 33rd AIAA Fluid Dynamics Conf. and Exhibit*
- Lentink D, Haselsteiner A F and Ingersoll R 2015 *In vivo* recording of aerodynamic force with an aerodynamic force platform: from drones to birds *J. R. Soc. Interface* **12** 20141283
- Liu T, Wang S, Zhang X and He G 2015 The lift problem in flapping forward flight at low reynolds numbers *53rd AIAA Aerospace Sciences Meeting*
- McGreevy P and Boakes R 2011 *Carrots and Sticks: Principles of Animal Training* (Sydney: Darlington Press)
- Minotti F O 2011 Determination of the instantaneous forces on flapping wings from a localized fluid velocity field *Phys. Fluids* **23** 111902
- Mohebbian A and Rival D E 2012 Assessment of the derivative-moment transformation method for unsteady-load estimation *Exp. Fluids* **53** 319–30
- Muijres F T, Bowlin M S, Johansson L C and Hedenström A 2012b Vortex wake, downwash distribution, aerodynamic performance and wingbeat kinematics in slow-flying pied flycatchers *J. R. Soc. Interface* **9** 292–303
- Muijres F T, Johansson L C, Barfield R, Wolf M, Spedding G R and Hedenström A 2008 Leading-edge vortex improves lift in slow-flying bats *Science* **319** 1250–3
- Muijres F T, Johansson L C and Hedenström A 2012a Leading edge vortex in a slow-flying passerine *Biol. Lett.* **8** 554–7
- Muijres F T, Johansson L C, Winter Y and Hedenström A 2011b Comparative aerodynamic performance of flapping flight in two bat species using time-resolved wake visualization *J. R. Soc. Interface* **8** 1418–28
- Muijres F T, Johansson L C, Winter Y and Hedenström A 2014 Leading edge vortices in lesser long-nosed bats occurring at slow but not fast flight speeds *Bioinspiration Biomimetics* **9** 025006
- Muijres F T, Spedding G R, Winter Y and Hedenström A 2011a Actuator disk model and span efficiency of flapping flight in bats based on time-resolved PIV measurements *Exp. Fluids* **51** 511–25

- Noca F, Shiels D and Jeon D 1997 Measuring instantaneous fluid dynamic forces on bodies, using only velocity fields and their derivatives *J. Fluids Struct.* **11** 345–50
- Noca F, Shiels D and Jeon D 1999 A comparison of methods for evaluating time-dependent fluid dynamic forces on bodies, using only velocity fields and their derivatives *J. Fluids Struct.* **13** 551–78
- Ol M V 2010 Unsteady low Reynolds number aerodynamics for micro air vehicles (MAVs) *Air Force Research Laboratory AFRL-RB-WP-TR-2010-3013*
- Pope S B 2000 *Turbulent Flows* (Cambridge : Cambridge University Press)
- Rosén M, Spedding G R and Hedenström A 2007 Wake structure and wingbeat kinematics of a house-martin *Delichon urbica* *J. R. Soc. Interface* **4** 659–68
- Rosenfeld M, Katija K and Dabiri J O 2009 Circulation generation and vortex ring formation by conic nozzles *J. Fluids Eng.* **131** 091204
- Sane S P 2003 The aerodynamics of insect flight *J. Exp. Biol.* **206** 4191–208
- Shyy W, Aono H, Kang C-K and Liu H 2013 *An Introduction to Flapping Wing Aerodynamics* (New York: Cambridge University Press)
- Shyy W, Lian Y, Tang J, Viiaru D and Liu H 2008 *Aerodynamics of Low Reynolds Number Flyers* (New York: Cambridge University Press)
- Skinner B F 1938 *The Behavior of Organisms: An Experimental Analysis* (New York: Appleton-Century-Crofts)
- Spedding G R 1986 The wake of a jackdaw (*Corvus monedula*) in slow flight *J. Exp. Biol.* **125** 287–307
- Spedding G R, Rayner J M V and Pennycuik C J 1984 Momentum and energy in the wake of a pigeon (*Columba livia*) in slow flight *J. Exp. Biol.* **111** 81–102
- Spedding G R, Rosén M and Hedenström A 2003 A family of vortex wakes generated by a thrush nightingale in free flight in a wind tunnel over its entire natural range of flight speeds *J. Exp. Biol.* **206** 2313–44
- Tian X I, Iriarte-Diaz J, Middleton K, Galvao R, Israeli E, Roemer A, Sullivan A, Song A, Swartz S and Breuer K 2006 Direct measurements of the kinematics and dynamic of bat flight *Bioinspiration Biomimetics* **1** S10–8
- Waldman R M and Breuer K S 2012 Accurate measurement of streamwise vortices using dual-plane PIV *Exp. Fluids* **53** 1487–500
- Wang S, Zhang X, He G and Liu T 2013 A lift formula applied to low-Reynolds-number unsteady flows *Phys. Fluids* **25** 093605
- Wang S, Zhang X and He H 2015 Evaluation of lift formulas applied to low-Reynolds-number unsteady flows *AIAA J.* **53** 161–75
- Wolf M, Ortega-Jimenez V M and Dudley R 2013 Structure of the vortex wake in hovering Anna's hummingbirds *Proc. R. Soc. B* **280** 20132391
- Young J 2005 Numerical simulation of the unsteady aerodynamics of flapping airfoils *PhD Thesis* Univ. of New South Wales, School of Aerospace, Civil and Mechanical Engineering, Canberra, Australia

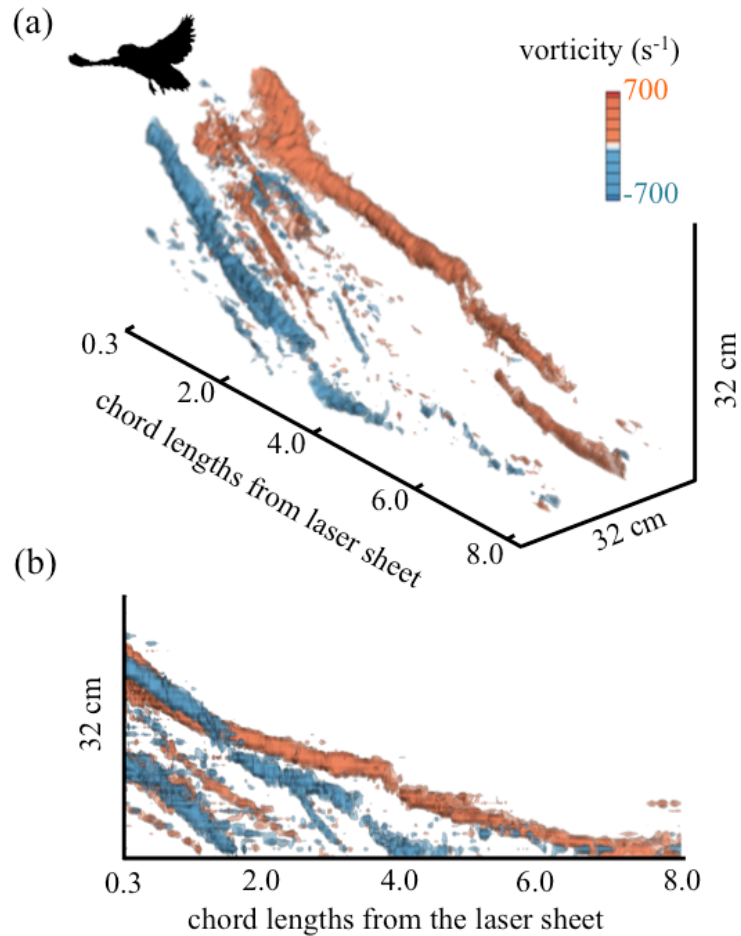


Figure 1. Wake measurements from a pilot study taken with the same experimental setup and similar flight conditions indicate that the vortex wake can become asymmetric. We checked the validity of the wake symmetry assumption by performing 2D PIV experiments with four PIV cameras during a pilot with a different parrotlet from the same colony. The fields of view of the cameras were distributed over both the width (2 cameras) and height (2 cameras) of the wake generated by the left and right wing. Here, we show the isosurfaces of vorticity in (a) an isometric view and (b) a side view. The isosurfaces show that the wingtip vortex from the left wing (blue isosurface) advects asymmetrically compared to the wingtip vortex from the right wing (red isosurface). The left and right wingtip vortices break down at different times, when the bird has traveled about 4 chord lengths past the laser sheet.

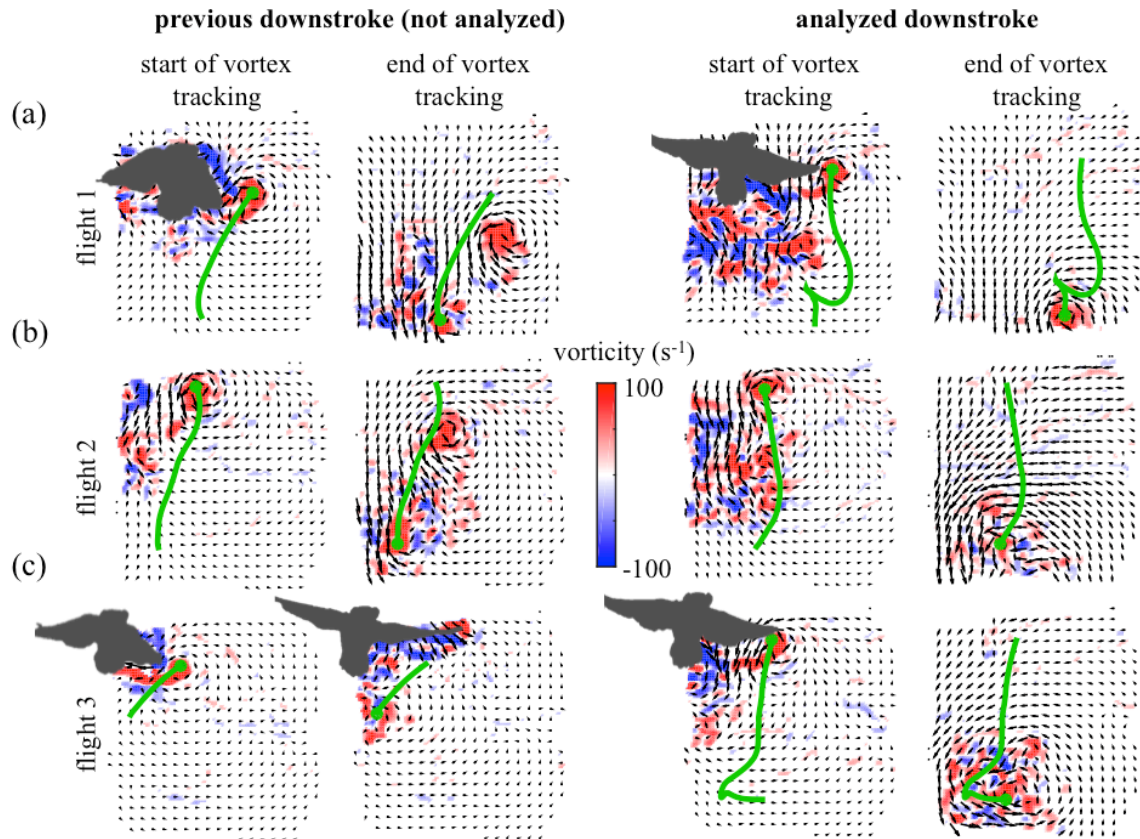


Figure 2. The tip vortex is visualized and tracked in the laser sheet for (a) flight 1, (b) flight 2, and (c) flight 3. The tracking reveals that two separate vortices are generated during two consecutive wingbeats: one at the end of the first downstroke (“previous downstroke”) and one near the middle of the second downstroke (“analyzed downstroke”). The positions of each vortex are shown at the start and end of tracking. The smoothed paths of the vortices are indicated in green. The vortex paths were smoothed with a moving average filter in MATLAB R2014B. The approximate position of the bird’s body and wings with respect to the field of view is shown as a gray silhouette. For all the vorticity fields without a silhouette, the bird was not in the field of view of the cameras. For flight 2, the bird flew at about 5 cm above the stereo field of view (estimated using the PIV cameras). This resulted in a reduced timeframe over which we could observe the vortex for flight 2, which is another reason why we selected flight 3 for in-depth discussion in the paper.

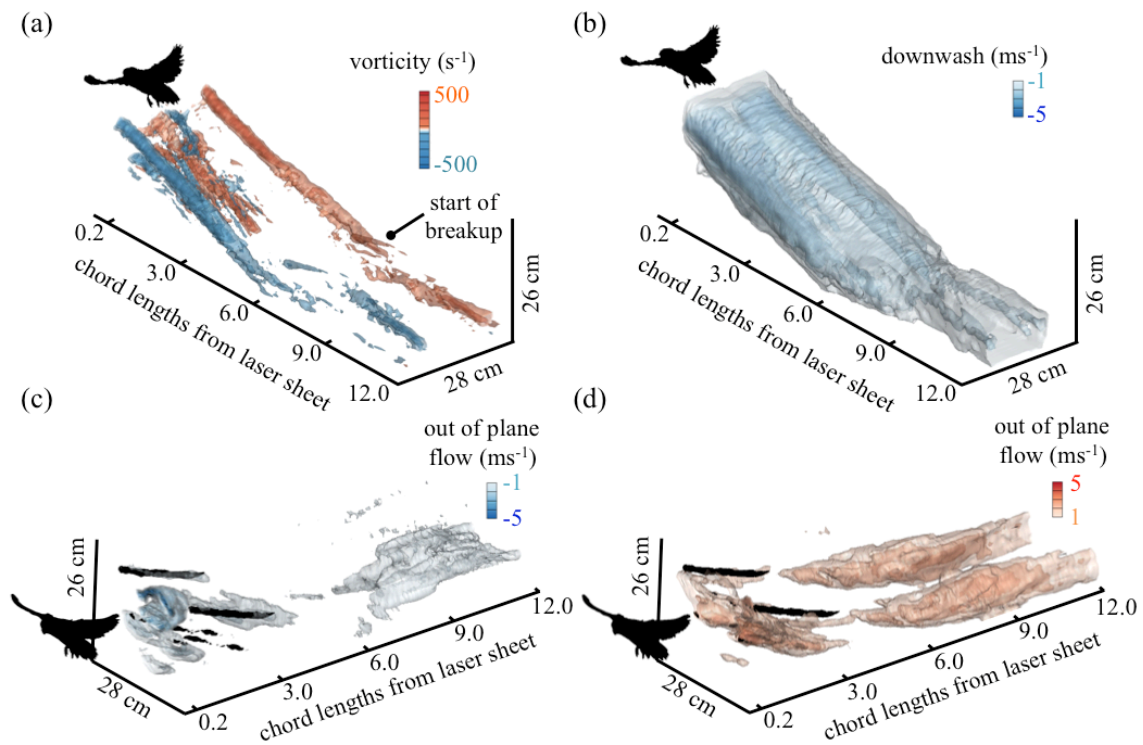


Figure 3. Shear corresponds with vortex breakdown in flight 1. (a) The strong tip vortices shed during mid-downstroke are visualized by vorticity isosurfaces. The vortex starts to break up after the bird has traveled about 5.5 chord lengths beyond the laser sheet. (b) The tip vortices are advected downwards by the strong downwash in the wake. (c) Isocontours of out-of-plane flow in the direction of the bird's flight show that there is out-of-plane flow in the vortex core in the direction of flight. The vortex core is indicated using a black vorticity isosurface ($\pm 350 \text{ s}^{-1}$). (d) Visualization of out-of-plane flow in the opposite direction of flight shows how a patch of out-of-plane flow advects next to the vortex core. This interaction results in a shear field composed of out-of-plane flow in opposing directions; the flow in the core of the vortex moves in the direction of flight, whereas the flow adjacent to the vortex moves in the opposite direction, away from the bird. In this shear field, the tip vortex breaks down and reconfigures into less-coherent vorticity patches that continue to interact (a).

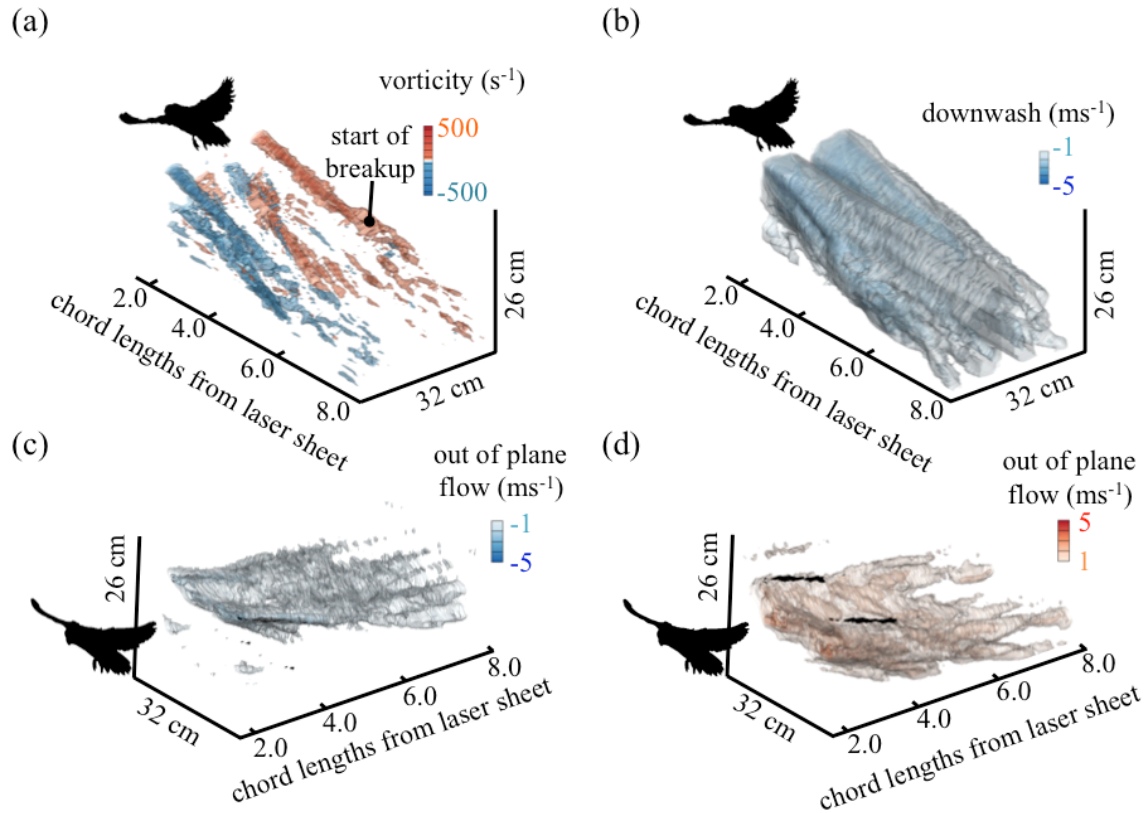


Figure 4. Shear corresponds with vortex breakdown in flight 2. Tracking of the wingtip vortex started later compared to the other two flights, because the bird in this flight flew a few centimeters above the field of view of the PIV cameras. (a) The strong tip vortices shed during mid-downstroke are visualized by vorticity isosurfaces. The vortex starts to break up after the bird has traveled about 6.6 chord lengths beyond the laser sheet. (b) The tip vortices are advected downwards by the strong downwash in the wake. (c) Isocontours of out-of-plane flow in the direction of the bird's flight show that there is out-of-plane flow in the vortex core in the direction of flight. The vortex core is indicated using a black vorticity isosurface ($\pm 350 \text{ s}^{-1}$). For this flight, there is more out of plane flow in the wake compared to the other two flights. (d) Visualization of out-of-plane flow in the opposite direction of flight shows that a large patch of out-of-plane flow advects next the vortex core. This interaction results in a shear field composed of out-of-plane flow in opposing directions; the flow in the core of the vortex moves in the direction of flight, whereas the flow adjacent to the vortex moves in the opposite direction, away from the bird. In this shear field, the tip vortex breaks down and reconfigures into less-coherent vorticity patches that continue to interact (a).

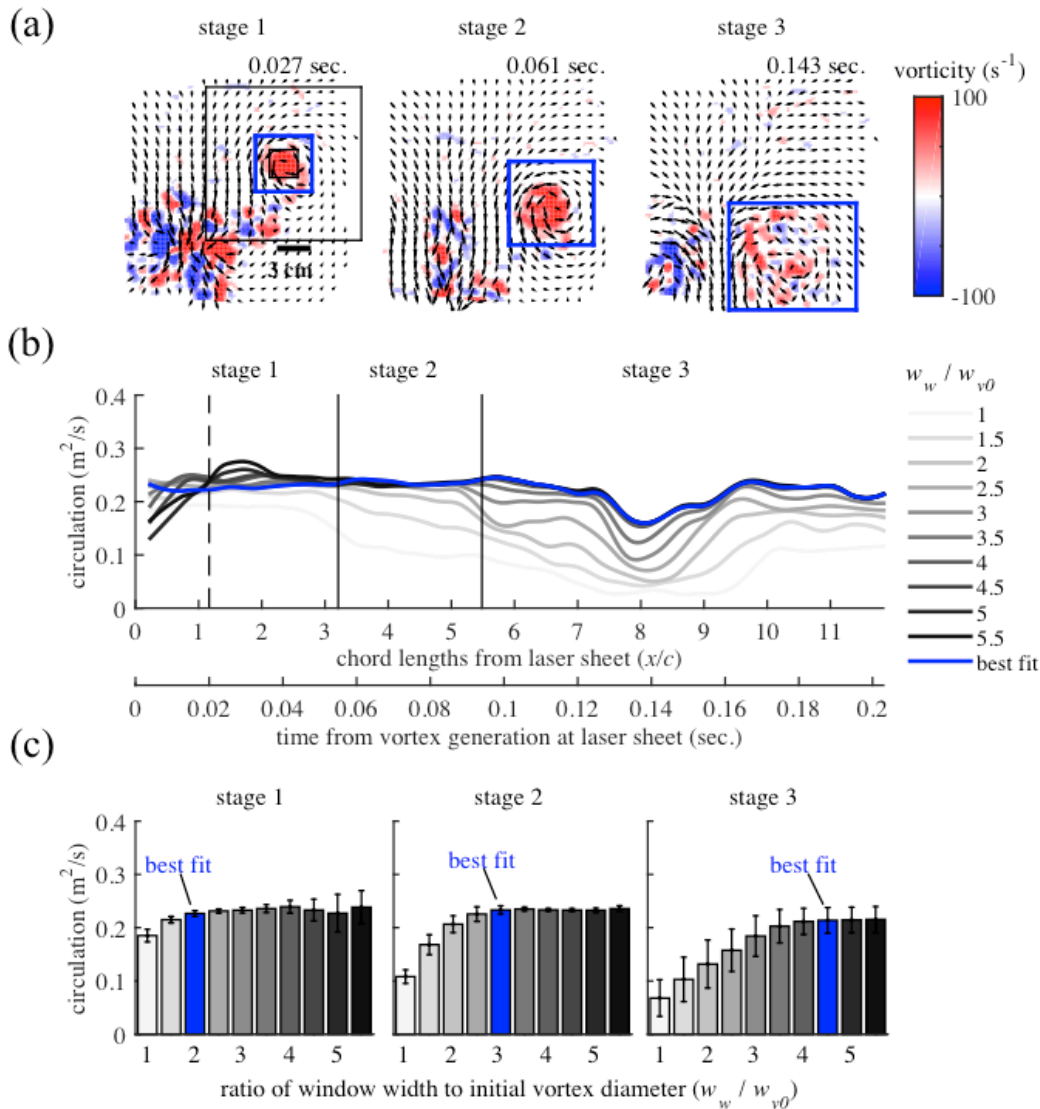


Figure 5. Wingtip vortex circulation of flight 1 is dependent on window size. (a) Integration of tip vortex circulation during vortex formation (stage 1), just before (stage 2), and after vortex breakdown (stage 3) shows that the optimal window size depends on vortex dynamics. (a) Snapshots of the velocity and vorticity field are shown at each of the three stages. The smallest and largest black box in the ‘stage 1’ plot show the range of integration domains considered. The best fit domain for each stage was determined by eye and is indicated in blue. (b) The calculated vortex circulation depends on window size and the time beyond vortex generation. As the vortex develops and breaks down, the integration window needs to be larger to capture the dispersed vorticity. The vertical dashed line indicates when the bird flew out of the laser sheet. The two solid vertical lines separate the vortex stages. (c) The average circulation as a function of integration window size is shown at each of the three stages. The larger windows capture more of the circulation for all three stages, but at the cost of a higher standard deviation in stage 1.

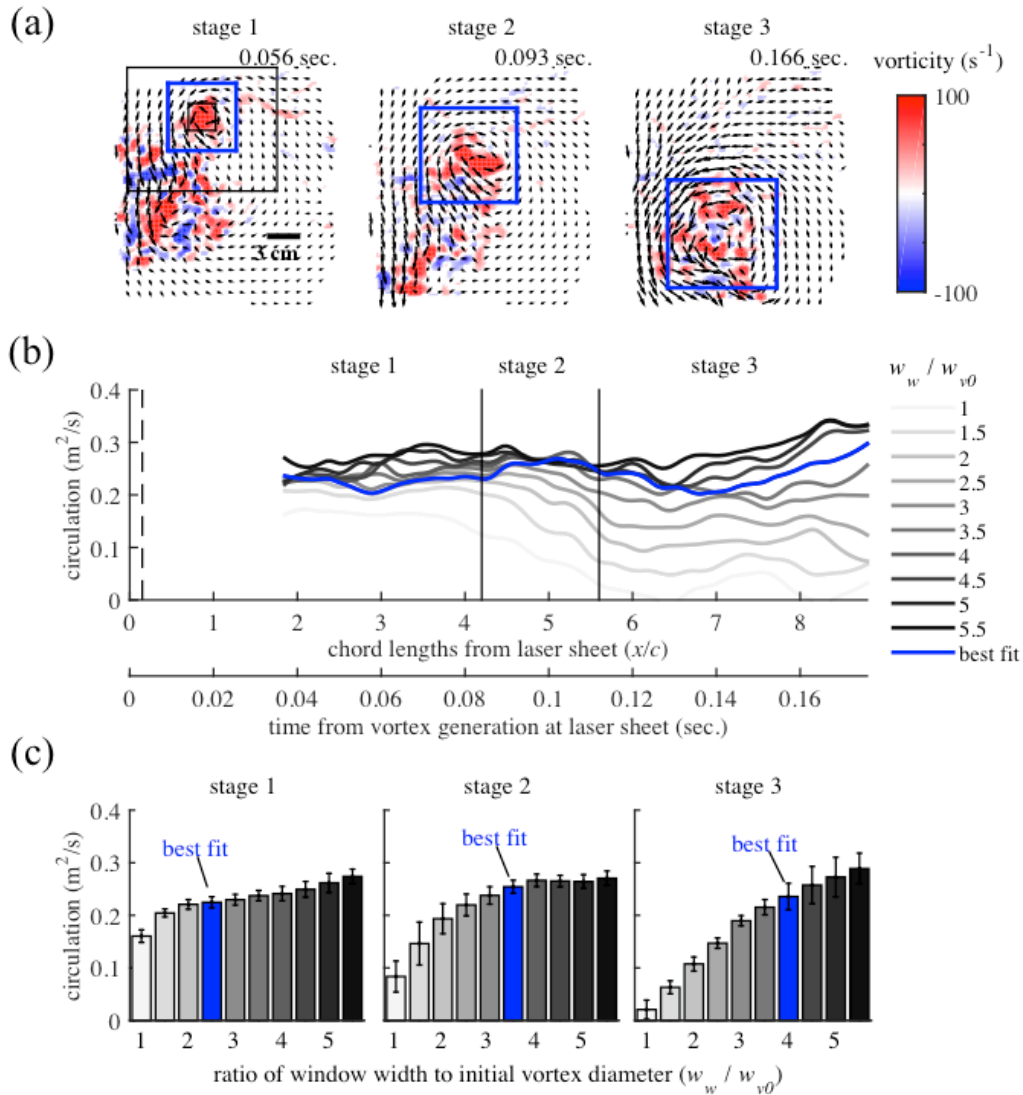


Figure 6. Wingtip vortex circulation of flight 2 is dependent on window size. (a) Integration of tip vortex circulation during vortex formation (stage 1), just before (stage 2), and after vortex breakdown (stage 3) shows that the optimal window size depends on vortex dynamics. (a) Snapshots of the velocity and vorticity field are shown at each of the three stages. The smallest and largest black box in the ‘stage 1’ plot show the range of integration domains considered. The best fit domain for each stage was determined by eye and is indicated in blue. (b) The calculated vortex circulation depends on window size and the time beyond vortex generation. As the vortex develops and breaks down, the integration window needs to be larger to capture the dispersed vorticity. The vertical dashed line indicates when the bird flew out of the laser sheet. The two solid vertical lines separate the vortex stages. (c) The average circulation is shown as a function of integration window size for each of the three stages. The largest window captures most of the circulation for all three stages. For this flight, the largest window in stage 1 yielded an elevated circulation average, but not a higher standard deviation.

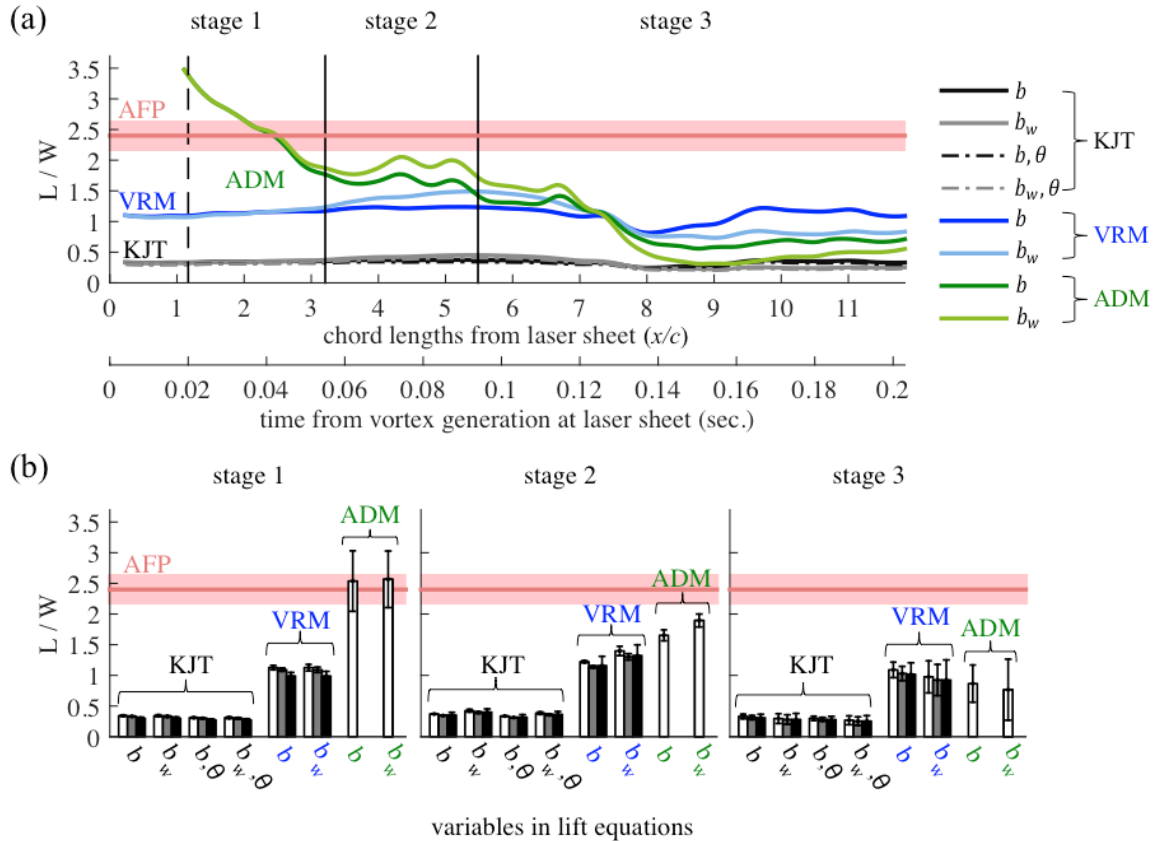


Figure 7. The calculated weight support for flight 1 varies depending on the model used. The aerodynamic lift predicted by the three models depends on parameter selection and the time passed after vortex generation. Beyond stage 1, all three models predict lower lift based on the flow generated during mid-downstroke than measured using an aerodynamic force platform (AFP) for parrotlets flying over 0.75 m. (a) The lift predicted by the KJT is less than half of that predicted by the VRM, both with and without multiplication with the cosine of stroke angle, θ , for KJT. Lift calculations based on mid-downstroke wingspan in the laser sheet, b , versus the span of the wake, b_w , diverge in stages 2 and 3. The wake span increases and then decreases as the vortex advects down. The lift predicted by the ADM best approximates the directly measured weight support with the AFP during stage 1. During stages 2 and 3, however, the downwash advects faster than the vortices, resulting in an underestimate of the lift during vortex breakdown and reorganization. The dashed line indicates when the bird flew out of the laser sheet; note that ADM could not be applied before. (b) The average lift within each stage calculated with the KJT and VRM is practically independent of the vorticity filtering technique (white bar, no thresholding; gray bar, vorticity cut-off filter; black bar, cut-off filter with Gaussian tail correction for each vortex).

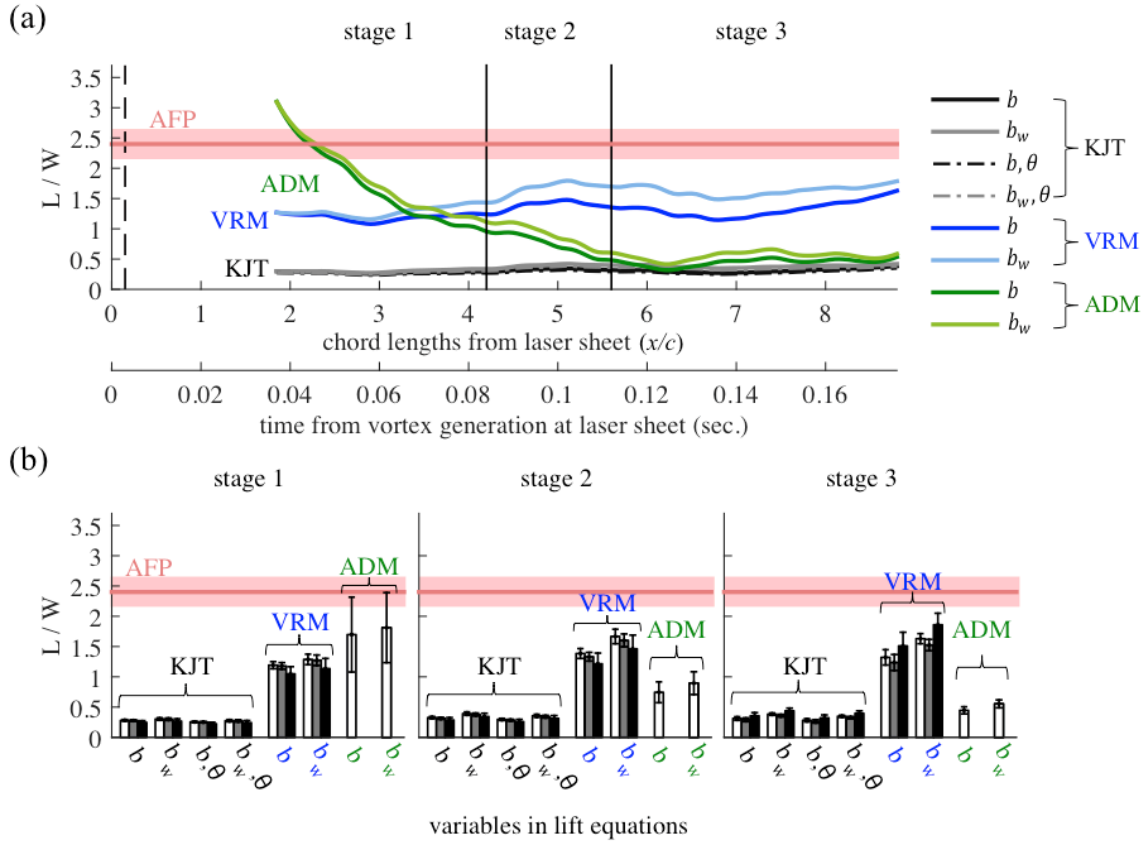


Figure 8. The calculated weight support for flight 2 varies depending on the model used. The aerodynamic lift predicted by the three models depends on parameter selection and the time passed after vortex generation. Beyond stage 1, all three models predict lower lift based on the flow generated during mid-downstroke than measured using an aerodynamic force platform (AFP) for parrotlets flying over 0.75 m. (a) The lift predicted by the KJT is less than half of that predicted by the VRM, both with and without multiplication with the cosine of stroke angle, θ , for KJT. Lift calculation based on mid-downstroke wingspan in the laser sheet, b , versus the span of the wake, b_w , diverges. The wake span increases as the vortex advects down, contrary to flight 3, which results in an increase in lift if the wake span is used. The lift predicted by the ADM best approximates the directly measured weight support with the AFP during stage 1. However, the downwash advects faster than the vortices, resulting in an underestimate of the lift during vortex advection and breakdown. The start of vortex tracking occurred when the vortex came into the field of view from above. (b) The stage-averaged lift calculated with KJT and VRM is practically independent of the vorticity filtering technique (white bar, no thresholding; gray bar, vorticity cut-off filter; black bar, cut-off filter with Gaussian tail correction for each vortex).